Chapter 8

Corrosion by Sulphur

8.1 INTRODUCTION

Sulphur is a relatively strong corrodent (or oxidising agent) as seen from the free energies of metal sulphide formation shown in Table 8.1. It is frequently present in fossil fuels and causes special forms of corrosion in petroleum and petrochemical processes based on these feedstocks, as well as in combustion

TABLE 8.1 Metal Sulphide Formation Free Energies

Reaction	T (°C)	$\Delta G^\circ = A + BT$ (J mol^{-1})		References
		A	B	
$Fe + \frac{1}{2}S_2 = FeS$	138–1190	−148,530	52.8	[1]
$\frac{9}{8}Co + \frac{1}{2}S_2 = \frac{1}{8}Co_9S_8$	<780	−165,770	83.28	[1]
$\frac{4}{3}Co + \frac{1}{2}S_2 = \frac{1}{3}Co_4S_3$	780–880	−129,490	50.04	[1]
$Co_9S_8 + \frac{1}{2}S_2 = 9CoS$	460–835	Not linear with T		[1]
$\frac{3}{2}Ni + \frac{1}{2}S_2 = \frac{1}{2}Ni_3S_2$	460–535	−165,560	78.03	[1]
$\frac{3}{2}Ni + \frac{1}{2}S_2 = \frac{1}{2}Ni_3S_{2-x}$	535–650	−140,080	34.94	[1]
$2Ni_3S_2 + \frac{1}{2}S_2 = Ni_6S_5$	400–525	−102,840	40.71	[1]
$Ni_3S_{2+x} + \frac{1}{2}S_2 = 3NiS$	560–810	−159,540	118.74	[1]
$Ni_6S_5 + \frac{1}{2}S_2 = 6NiS$	400–560	−111,920	62.93	[1]
$Cr + \frac{1}{2}S_2 = CrS$	900–1100	−204,060	56.8	[2,3]
$3CrS + \frac{1}{2}S_2 = Cr_3S_4$	700–900	−226,170	169	[3]
$2Cr_3S_4 + \frac{1}{2}S_2 = 3Cr_2S_3$	600–900	−42,719	52.0	[3]
$Mn + \frac{1}{2}S_2 = MnS$	<1244	−263,380	60	[4]
$\frac{2}{3}Mo + \frac{1}{2}S_2 = \frac{1}{3}Mo_2S_3$	700–1100	−179,430	75.9	[5]
$Mo_2S_3 + \frac{1}{2}S_2 = 2MoS_2$	700–1100	−179,720	82.2	[5]

High Temperature Oxidation and Corrosion of Metals. http://dx.doi.org/10.1016/B978-0-08-100101-1.00008-X

processes. Because metal sulphides are very different from the corresponding oxides, corrosion by sulphur is generally much more rapid and merits separate consideration. Three situations are of interest: oxidising environments in which sulphur is a minority species, reducing environments where sulphur is the principal corrodent and molten sulphate salt environments which form in the presence of alkali and some other metals. The first form of sulphur corrosion was discussed in Chapter 4, and we focus here on sulphidation under reducing conditions and molten salt induced attack, commonly described as 'hot corrosion'.

8.2 SULPHIDATION OF PURE METALS

The sulphidation of metals and alloys has been reviewed several times [6–9], most recently by Mrowec [10]. The widespread adoption of catalytic reforming and hydrodesulphurising processes in the petroleum industry produced a need for improved sulphidation resistance at moderate temperatures. A renewed interest in coal gasification as a route to more efficient electric power generation has led to a number of processes, most of which have in common high temperatures and substantial concentrations of gaseous sulphur under reducing conditions [10,11]. Each of these technological changes led to a substantial research effort which has generated a reasonably good level of understanding. Unfortunately, however, the goal of a practical alloy possessed of superior intrinsic sulphidation resistance has proven elusive.

8.2.1 Sulphidation Kinetics and Rates

Provided that liquid sulphide formation is avoided, most metal sulphide scales grow according to parabolic kinetics, reflecting rate control by solid-state diffusion. However, the rate constants are, for most metals, extraordinarily high (Table 8.2), and much faster than for the analogous metal oxidation reactions (Table 3.1). It is noted in particular that the sulphidation rate of chromium is four to five orders of magnitude faster than the corresponding oxidation rate. It is evident that the major constituents of many heat-resisting alloys are, on this basis, predicted not to form protective scales.

Examining Table 8.2 further, it is observed that MnS scales grow much more slowly than the sulphides formed on Fe, Ni and Co. In fact, manganese sulphidises more slowly than chromium. Even slower growing scales are formed on the refractory metals Mo, W, Ta and Nb. The sulphidation rates observed for these metals are quite acceptable, being of the same order of magnitude as the rate of chromium oxidation [10]. This is quite unlike the oxidation performance of these metals: molybdenum and tungsten react to form volatile oxides; titanium and niobium dissolve oxygen and grow porous, nonprotective oxides according to fast linear kinetics. These different patterns

TABLE 8.2 Sulphidation Rate Data

Metal	T (°C)	p_{S_2} (atm)	E_A (kJ mol^{-1})	n	k_w (g^2 cm^{-4} s^{-1})[a]	References	k_w (S)/k (O)[b]
Fe	650–750	1	92			[12]	10^2
	700–850	0.26	84	5.6	1×10^{-5}	[13,14]	
	650–900	0.13	70	6		[15]	
	600–1000	10^{-4}	61			[16]	
		10^{-8}	12				
	527–697	2×10^{-6}	26	5.5		[17]	
Co	650–800	1	142		3×10^{-6}	[18]	450
	500–700	0.013	78	2.5		[19]	
	800–1000	2×10^{-2}	210			[20]	
Mn	800–1000	10^{-8}–10^{-4}	82–96	5.8–6.3		[21]	≈1
	700–1000	1	130		4×10^{-9}	[22]	
	550–711	5×10^{-9}–4×10^{-3}	72	6.2		[23]	
Ni	420–640	1	92		8×10^{-7} (600°C)	[24]	10^5 (600°C)
Cr	800–1000	1	192		3×10^{-8}	[25]	$>10^4$
	700–900	1	72		1×10^{-7}	[26]	
Ta	800–1000	1	94		7×10^{-10}	[27]	
Mo	850–1050	50% H_2S	199		8×10^{-11} (900°C)	[28]	
	700–950	1.3×10^{-3}	147		7×10^{-12}	[29]	
W	380–980	50% H_2S	135		3×10^{-10}	[28]	
Nb	800–1200	1	58		10^{-13}	[27]	

[a] *Rate at 800°C, $p_{S_2} = 1$ atm, unless otherwise noted.*
[b] *Ratio of rate constants for sulphidation and oxidation, 800°C, unless otherwise noted.*

of behaviour can be understood from a brief examination of metal sulphide and oxide solid-state chemistry.

The general properties of transition metal sulphides have been reviewed by Rao and Pisharody [30], and their nonstoichiometry, lattice defects and transport properties by Halstead [31], Mrowec and Przybylski [9] and Mrowec [10]. Because the sulphide ion is so much larger than the oxide (diameter 0.368 nm compared with 0.28 nm), the cation/anion radius ratios in metal oxides are smaller than in the corresponding sulphides, leading to different crystal structures. Whereas simple oxides, MO, are usually cubic, monosulphides usually adopt the NiAs structure, in which the sulphide ions occupy a hexagonal lattice. All of the chromium sulphides (CrS, Cr_3S_4 and Cr_2S_3 at high temperature) can be regarded as defective NiAs structures [32,33]. The difference in anion size leads also to M-S bond lengths longer than the corresponding M-O distances. In ionic crystals, this leads to smaller lattice energies for the sulphides. This is reflected in the lower free energies for the sulphide formation (Tables 2.1 and 8.1) and in the generally lower melting points of sulphides. The low melting metal/metal sulphide eutectic temperatures shown in Table 8.3 set rather restrictive upper temperature service limits for some metals.

The low stabilities of the sulphides means that point defects are easily created and, as seen from Eq. [3.19], deviation from stoichiometry is more easily produced. The NiAs structure sulphides of Fe, Co, Ni and Cr are seen in Table 8.3 to display large deviations from stoichiometry. In this structure, the point defect species are predominantly cationic, either vacancies or supernumerary cations occupying otherwise empty octahedral sites between the

TABLE 8.3 Metal/Metal Sulphide Eutectic Temperatures and Sulphide Nonstoichiometry Ranges

System	T_E (°C)	Sulphide (T (°C))	δ	References
Fe/FeS	988	$Fe_{1-\delta}S$ (800)	0 to 0.20	[1]
Co/Co_4S_3	880	$CoS_{1+\delta}$ (800)	0 to 0.07	[1]
Ni/Ni_3S_2	645	$Ni_3S_{2\pm\delta}$ (645)	−0.188 to 0.222	[1]
Mn/MnS	1242	$Mn_{1-\delta}S$ (800)	0 to 1×10^{-4}	[34]
		$Cr_{1-\delta}S$ (700)	0.032 to 0.205	[3]
		$Cr_{3\pm\delta}S_4$ (700)	−0.10 to 0.11	[35]
		$Cr_{2+\delta}S_3$ (700)	0.054 to 0.11 (tr)	[3]
			0.033- (rh)	

hexagonally close-packed sulphur anions. The much lower nonstoichiometry of MnS is associated with its cubic structure and somewhat greater stability.

8.2.2 Growth of NiAs-Type Sulphide Scales

In their extensive review of pure metal sulphidation reactions, Mrowec and Przybylski [9] demonstrate that the NiAs structure sulphides invariably grow by outward metal diffusion. The high-defect densities of the simple metal sulphides imply high diffusion rates and consequently rapid sulphide scaling. As shown in Section 3.7, Wagner's diffusion model provides a quantitatively successful description of iron sulphidation. This is one of the few systems, and the only sulphidation reaction, for which sufficient information is available to perform such a calculation. The important conclusion to be drawn is that iron sulphide scale growth is supported by lattice diffusion even at quite low temperatures. It seems likely that this will be true also for other reactions forming sulphides with the NiAs structure.

Sulphidation and oxidation rates, k_w, are compared in Table 8.2 for metals which form NiAs-type sulphides. Although weight uptake rates reflect the different atomic weights of sulphur and oxygen, the effect is approximately compensated by the difference in compound densities, when scaling rates, k_p, are calculated from Eq. [1.18] or [1.32]. It is seen that Fe, Co, Ni and Cr all sulphidise faster than they oxidise at 800°C. The difference in the case of iron is not so large, reflecting the similar values of δ in $Fe_{1-\delta}O$ and $Fe_{1-\delta}S$, and a higher D_v in the sulphide (Section 3.7). Data for nickel corrosion are provided for $T = 600$°C, below the eutectic temperature for the Ni-S system. Nickel sulphidation is extraordinarily rapid, reflecting the high δ values of nickel sulphides (Table 8.3) and the high-defect mobilities in these compounds. Importantly, for heat-resisting alloys, chromium sulphidises much more rapidly than it oxidises, again reflecting the difference between widely non-stoichiometric chromium sulphides and closely stoichiometric Cr_2O_3.

8.2.3 Sulphidation of Manganese

Manganese is unusual in having similar sulphidation and oxidation rates. Activation energies for the two processes are also rather similar: 88 kJ mol^{-1} for sulphidation [21,36] and 81 kJ mol^{-1} for oxidation [37]. These similarities come about as a result of the unusual cubic structure of α-MnS, its small deviation from stoichiometry (Table 8.3) and the fact that manganese vacancies are the mobile defects in both oxide and sulphide. Of the common metals for which data are available, only manganese provides anything like acceptable sulphidation resistance. Its sulphidation rate constant is nonetheless about four orders of magnitude faster than that of chromium oxidation at 800°C, implying the need for a corrosion allowance about 100 times larger.

8.2.4 Sulphidation of Refractory Metals

The refractory metals for which data are available appear to provide superior sulphidation resistance, as seen from the low scaling rates in Table 8.2. In seeking to explain this phenomenon, Mrowec and Pryzbylski [9] speculated that these sulphides, like the refractory metal oxides, might be anion diffusers. In this event, the large size of the sulphide ion might explain its low mobility. This reasoning appears to be correct for molybdenum and tungsten sulphides, which have been shown in marker experiments [28] to grow by slow inward sulphur transport. The molybdenum sulphide is closely stoichiometric, with a maximum value of $\delta < 8 \times 10^{-5}$ in $MoS_{2\pm\delta}$ between 900 and 1100°C, although some sulphur disorder ($\delta \leq 10^{-3}$) can be achieved via stacking faults [38]. However, subsequent investigations of nonstoichiometry in other refractory metal sulphides have revealed high defect densities in the cation sublattices.

Many of the refractory metal disulphides, MS_2, have the $Cd(OH)_2$ structure, made up of 'sandwiches' consisting of two planes of sulphide ions with a plane of cations between them [30]. These sandwiches are stacked along the c axis of a hexagonal lattice to form the crystal structure. The spaces between the sandwiches are available for occupancy by additional metal, forming lower sulphides. Thus, for example, Nb_2S_3 can be regarded in a structural sense as $Nb_{1+x}S_2$ [39] and a similar description applies to the Ti-S system [40]. The ability of these structures to accommodate different metal-sulphur ratios permits substantial deviations from stoichiometry, the defects lying within the cation sublattices. Thus the high-temperature niobium sulphide NbS_ν exists over the range $1.4 \leq \nu \leq 1.7$ at 1000°C [41]. A defect model based on metal vacancies and interstitials [42] was shown to fit the relationship between y and p_{S_2} at 1000°C, and at other temperatures when point defect charges are taken into account [43]. Gesmundo et al. [43] have shown that this model matches the sulphur partial pressure dependence of k_p for growth of this sulphide on niobium, if both defect species contribute to diffusion. The rather slow growth rates thus reflect very low defect mobilities.

Titanium forms a series of sulphides between TiS (with a NiAs structure) and TiS_2 (with a $Cd(OH)_2$ structure [39]). Like the niobium sulphides, the titanium compounds also evidence large departures from stoichiometry. Saeki and Onoda [44] found compositional ranges for TiS_ν of $1.57 < \nu < 1.72$ and $\nu > 1.82$ at 950°C and high sulphur potentials. There appears to be no information available for pure titanium metal sulphidation rates.

8.3 ALLOYING FOR SULPHIDATION PROTECTION

A large research effort has been devoted to the search for sulphidation-resistant alloys [7–10]. Almost all of this work was based on the design strategy which has proved so successful for oxidation resistance: selective

reaction of an alloy constituent to form a slow-growing protective scale. For such a strategy to succeed, the following conditions must be met:

1. The selected metal must have a sulphide much more stable than the alloy solvent metal, so that moderate alloying levels will suffice.
2. The selected metal sulphide must grow slowly.
3. The preferentially formed sulphide must act as a barrier to outward diffusion of other alloy components.

There are other requirements concerning the physical and mechanical properties of the alloy and scale, but an alloy satisfying just the basic requirements has yet to be developed.

8.3.1 Alloying With Chromium

The difficulty of meeting the first requirement is illustrated in Fig. 8.1. Comparison with analogous data for oxide formation (Fig. 2.1) shows that the differences between free energies of formation of different metal sulphides are less than for the corresponding oxides. Consider the competition between chromium and iron sulphide formation:

$$\mathrm{Cr} + \mathrm{FeS} = \mathrm{CrS} + \mathrm{Fe} \qquad [8.1]$$

$$\Delta G_1^\circ = -55,530 + 3.95\,T\ \mathrm{J\ mol^{-1}} \qquad [8.2]$$

At 700°C, $\Delta G_1^\circ = -52$ kJ mol^{-1}, and therefore, in the case of pure, immiscible sulphide phases

$$\frac{a_{\mathrm{Fe}}}{a_{\mathrm{Cr}}} = K_1 = 595 \qquad [8.3]$$

In an ideal Fe-Cr solid solution, the minimum concentration of N_{Cr} for CrS formation is therefore 0.16%. This is much higher than the value of N_{Cr} required (<1 ppm) to thermodynamically stabilise Cr_2O_3 with respect to FeO on an Fe-Cr alloy (Section 2.4), but nonetheless a promising level. Unfortunately, the assumption of immiscible sulphide phases is a poor one, as seen from the Fe-Cr-S phase diagram in Fig. 8.2. A minimum chromium concentration of 6 wt% ($N_{\mathrm{Cr}} = 0.064$) is required to stabilise the $(\mathrm{Cr,Fe})_{1-\delta}\mathrm{S}$ phase with respect to the $(\mathrm{Fe,Cr})_{1-\delta}\mathrm{S}$.

Selective reaction of chromium depletes the alloy subsurface region. Diffusion paths observed for an 18.5 wt% Cr steel after sulphidation are mapped on the phase diagram of Fig. 8.2 to illustrate the effect: As the value of $N_{\mathrm{Cr}}^{(\mathrm{o})}$ is increased, a degree of protection is achieved, as greater amounts of chromium-rich sulphide $(\mathrm{Cr,Fe})_3\mathrm{S}_4$ are formed [50–52]. However, an additional layer of $(\mathrm{Cr,Fe})_{1-\delta}\mathrm{S}$ grows on top of the $(\mathrm{Cr,Fe})_3\mathrm{S}_4$. Data from Narita and Nishida for a reaction at $p_{\mathrm{S}_2} = 1$ atm are shown in Fig. 8.3. The reductions in rate achieved by chromium additions are relatively small and decrease with

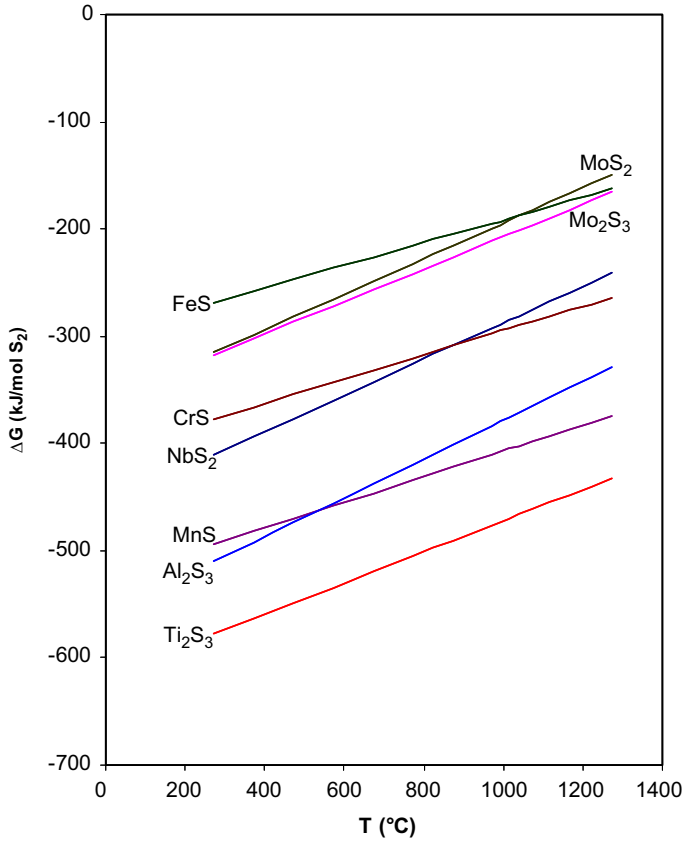

FIGURE 8.1 Ellingham diagram for selected sulphides. *Data sources: CrS (P. Hagan, J.F. Elliott, Trans. AIME 239 (1967) 513), FeS (T. Rosenqvist, J.I.S.I. 176 (1954) 37), Mo-S (T.R. Stubbles, F.D. Richardson, Trans. Faraday Soc. 56 (1960) 1460), Ti_2S_3 (M. Saeki, M. Onoda, J. Less, Common Met. 108 (1985) 327), MnS (O. Kubaschewski, C.B. Alcock, P.J. Spencer, Materials Thermochemistry, sixth ed., Pergamon, Oxford, 1993), Al_2S_3 (B. Pei, T. Rosenqvist, Scan. J. Met. 20 (1991) 331; M.J. Ferrante, J.M. Stuve, H.C. Ko, R.R. Brown, High Temp. Sci. 14 (1981) 91), NbS_2 (S.R. Shatynski, Oxid. Met. 11 (1977) 307).*

increasing temperature. This is a consequence of, firstly, the rather rapid rate of chromium sulphide growth (Table 8.2) and, secondly, its evidently high permeability for iron. Both effects result from the high concentration of cation defects in Cr_3S_4 [35]. It is noted that the phase diagram of Fig. 8.2 is inaccurate, as it omits this important phase.

Attempts to protect nickel by alloying with chromium are similarly limited in their success [26,53–56]. Again, the explanation is to be found in the high permeability of nickel in the chromium-rich sulphides and the rapid growth of the latter. The high solubility of nickel in chromium sulphides is evident in the phase diagrams of Fig. 8.4.

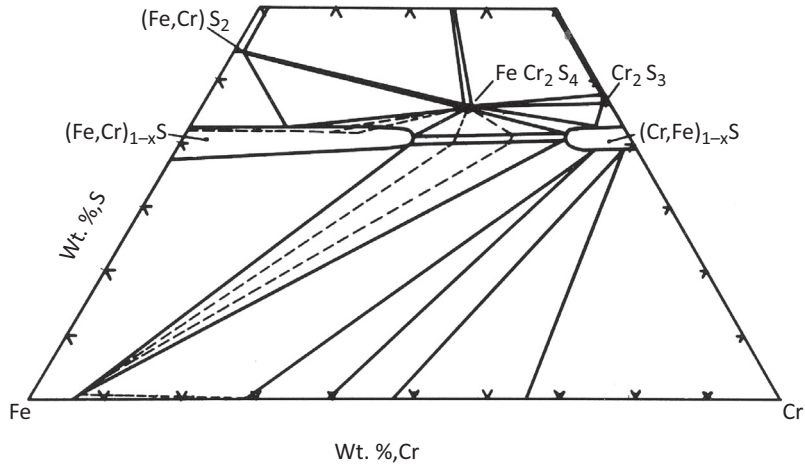

FIGURE 8.2 Fe-Cr-S isothermal section for 700°C [48], showing diffusion paths measured on sulphidised Fe-18.5 Cr-4.9 Ni-2.7 Mo stainless steel [49]. *With kind permission from Springer Science and Business Media.*

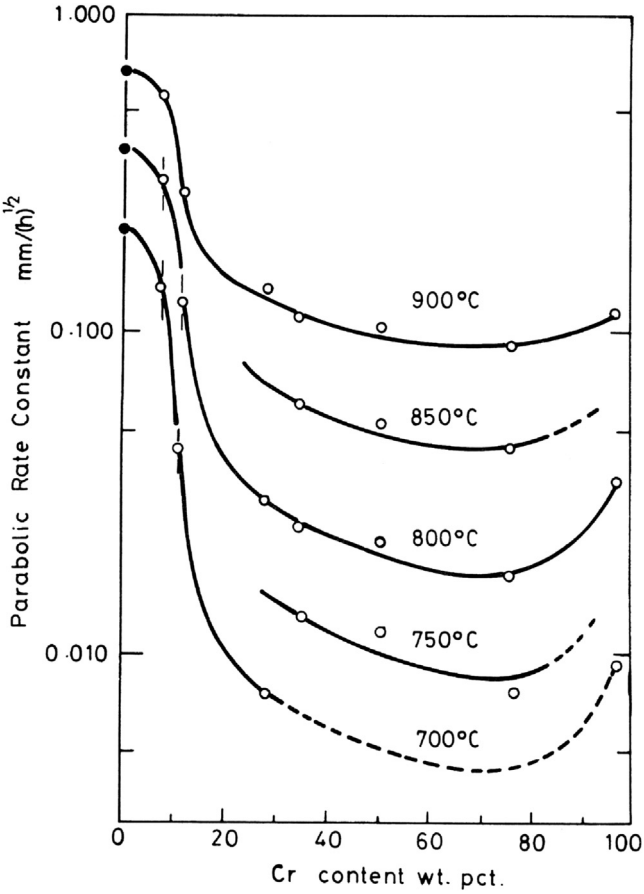

FIGURE 8.3 Sulphidation rates for Fe-Cr alloys reacted at $p_{S_2} = 1$ atm [52]. *With kind permission from Springer Science and Business Media.*

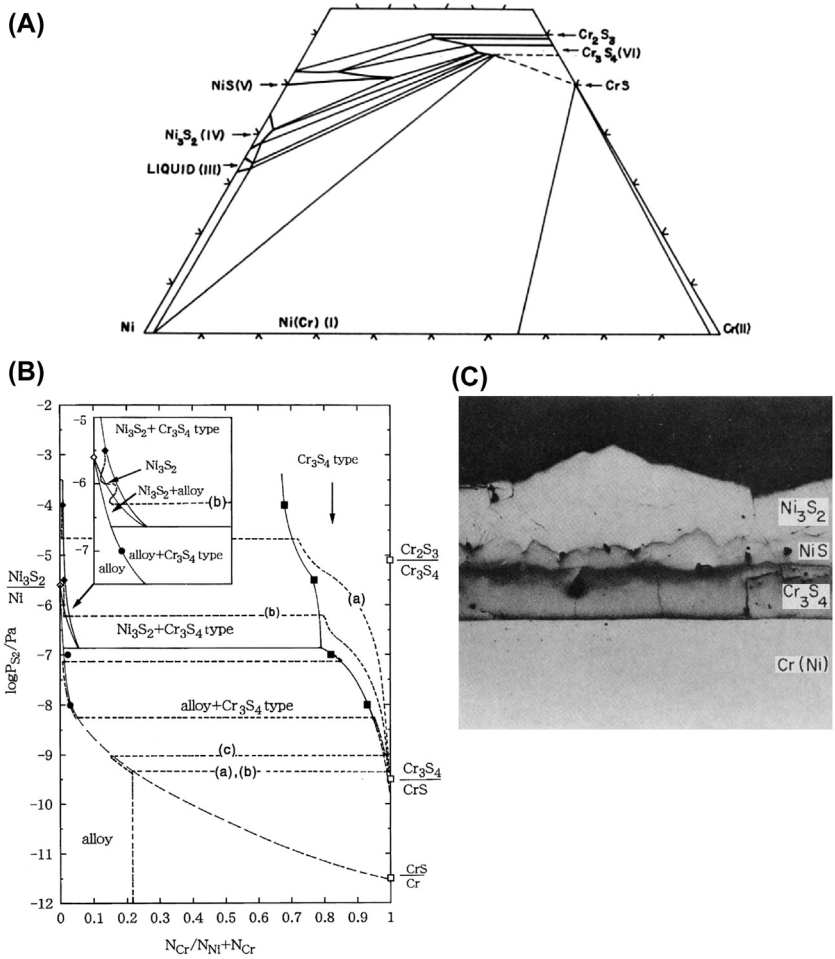

FIGURE 8.4 Phase equilibria in the Ni-Cr-S system: (A) isothermal section at 700°C *(with kind permission from J.S. Kirkaldy, G.M. Bolze, D. McCutcheon, D.J. Young, Met. Trans. 4 (1973) 1519, Springer Science and Business Media)*, (B) sulphur potential relationships at 600°C *(with kind permission from C. Fang, H. Yakuwa, M. Miyasaka, T. Narita, Oxid. Met. 54 (2000) 173, Springer Science and Business Media)* and (C) scale cross-section grown on Ni-20Cr at 700°C *(reproduced by G. Romeo, W.W. Smeltzer, J.S. Kirkaldy, J. Electrochem. Soc. 118 (1971) 1336; 119 (1972) 1267, permission of The Electrochemical Society).*

8.3.2 Alloying With Aluminium

Aluminium sulphide is considerably more stable than $Fe_{1-\delta}S$ and the nickel sulphides (Table 8.1, Fig. 8.1). The Fe-Al-S phase diagram at 750°C [58] shows, however, that a scale-alloy interface aluminium level $N_{Al,i} \approx 0.1$ is

required to stabilise Al_2S_3. This diagram also shows the existence of a ternary compound $FeAl_2S_4$, which has been shown [59,60] to be hexagonal in structure. Early work [61,62] indicated that Fe-Al alloys were much more resistant to sulphidation than Fe-Cr equivalents. Subsequent investigations [51,63–66] of Fe-Al alloy sulphidation have led to a diversity of reports on what is apparently a very complex system.

Alloys containing $N_{Al}^{(o)} = 0.1 - 0.2$ form duplex scales of $Fe_{1-\delta}S$ outside Al_2S_3 in the short term (Fig. 8.5). At higher N_{Al} levels, an intermediate layer of $FeAl_2S_4$ forms. However, as the reaction proceeds, internal Al_2S_3 precipitation develops, and a new layer of $Fe_{1-\delta}S$ forms beneath the Al_2S_3. Thus the Al_2S_3 layer fails to prevent outward iron diffusion and eventually fails also to prevent sulphur access to the underlying alloy. The discussion is hampered by a lack of information on the defect nature and diffusion properties of the aluminium-rich sulphides.

Aluminium additions to nickel are even less effective. Exposure of the intermetallic γ'-Ni_3Al to H_2/H_2S atmospheres at 875°C led to either Al_2O_3 formation if p_{S_2} was too low to stabilise a nickel sulphide, or liquid sulphide when p_{S_2} exceeded the $Ni/NiS_x(l)$ equilibrium value [67]. The β-NiAl intermetallic failed to provide selective aluminium sulphidation when exposed to high sulphur partial pressures [68].

Finally, it should be noted that Al_2S_3 and $FeAl_2S_4$ hydrolyse readily on exposure to air, producing $H_2S(g)$ and hydrated alumina. The latter disintegrates to a powder as a result of the volume expansion, and it seems unlikely that Al_2S_3 formation can ever provide a practical route to alloy protection.

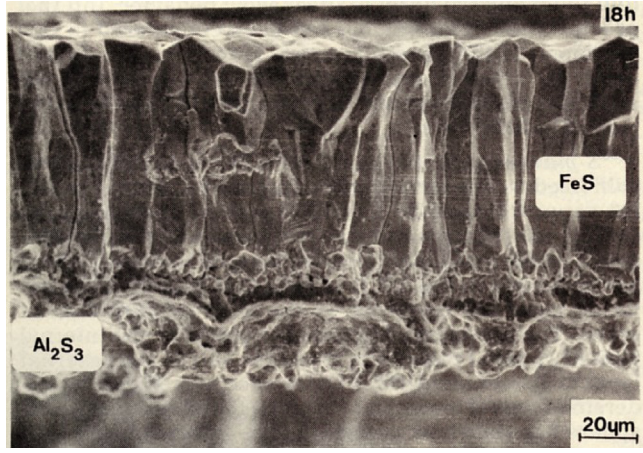

FIGURE 8.5 Fracture cross-section of sulphide scale grown on Fe-10 a/o Al at 750°C in H_2/H_2S [65]. *Reproduced by permission of The Electrochemical Society.*

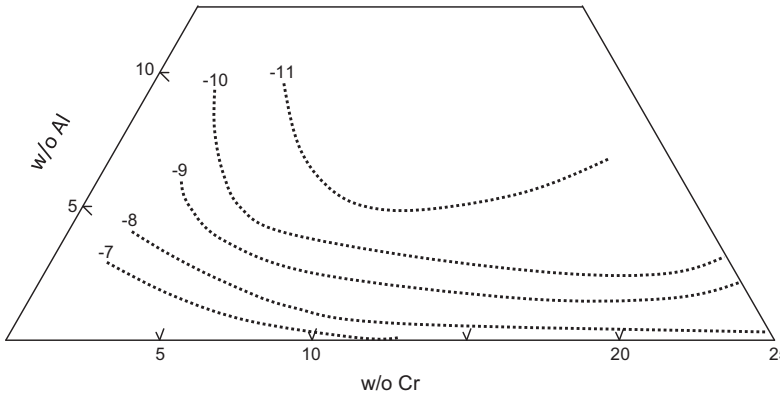

FIGURE 8.6 Iso-corrosion contours for Fe-Cr-Al alloys drawn from data due to Zelanko and Simkovich [70]. Numbers are values of $\log_{10} k_w$ at $T = 540°C$.

8.3.3 M-Cr-Al Alloys

The sulphidation resistance of Fe-Cr-Al alloys has been extensively explored. In 1961, Setterland and Prescott [62] reported that alloys containing both chromium and aluminium were highly resistant to low p_{S_2} atmospheres at 450°C. Mrowec and Wedrychowska [69] sulphidised alloys containing 18−25 wt% Cr and 1−5 wt% Al (and minority amounts of C, Mn and Ni) at temperatures of 800−1100°C and $p_{S_2} = 1$ atm. Parabolic kinetics were observed, and the presence of aluminium was found to decrease the rate. Duplex scales of coarse-grained $Fe_{1-\delta}S$ over a fine-grained, porous layer containing $Fe_{1-\delta}S$, chromium sulphides, $FeCr_2S_4$ and Al_2S_3 developed.

Zelanko and Simkovich [70] reacted a range of ternary alloys with H_2/H_2S mixtures corresponding to $p_{S_2} = 2 \times 10^{-11}$ at 540°C, obtaining parabolic kinetics in all cases. Their rate data are shown plotted as iso-corrosion contours on a composition triangle in Fig. 8.6, where a rather complex interaction between chromium and aluminium effects is evident. It is seen that a typical FeCrAl composition of Fe-20Cr-5Al would be expected to perform quite well under isothermal conditions, at this admittedly low temperature. Rates have been measured at 800°C for similar composition alloys as $\sim 5 \times 10^{-7}$ $g^2cm^{-4}s^{-1}$ at sulphur potentials of 1 atm [69] and 10^{-7} atm [71]. These values are to be compared with the rate constant for pure iron of $k_w \approx 10^{-5}$ g^2 cm^{-4} s^{-1} at this temperature.

Scale morphologies and constitutions were similar to those reported by Mrowec and Wedrychowska, except that the outer $Fe_{1-\delta}S$ layer was absent on higher alloys. The difference presumably reflects the difference in p_{S_2} values. At both sulphur potentials, the scale inner layers were always heterophase, reflecting the inability of these alloys to selectively to form a single-phase, protective layer. This failure is probably the result of both

thermodynamic and kinetic factors. The chromium-rich sulphides are not much more stable than the chromium-doped $(Fe,Cr)_{1-\delta}S$, and the same may be true of the aluminium-rich sulphides. The rapid rates at which all sulphides grow lead to high k_c values and strong depletion in the alloy subsurface zone (Eq. [5.25]), making selective sulphidation more difficult. Finally, the high growth rate of $Fe_{1-\delta}S$ impedes formation of a continuous, protective chromium and/or aluminium-rich sulphide.

The sulphidation of Ni-Cr-Al alloys at $p_{S_2} = 1$ atm and 680–950°C was reported [72] to proceed according to nonparabolic and rather irreproducible kinetics, perhaps indicating liquid nickel sulphide formation.

8.3.4 Alloying With Manganese

Nishida et al. [22,73] exposed iron-manganese alloys at temperatures of 700–1000°C to elemental $S_2(g)$ at 1 atm and to H_2/H_2S mixtures corresponding to p_{S_2} values of 10^{-11} to 10^{-2} atm. The kinetics were always parabolic, and large decreases in rate accompanied increases in manganese levels from 11 to 64 wt%. The protective effect was associated with the formation of a Mn(Fe)S layer at the scale-alloy interface. An induction period observed in H_2/H_2S atmospheres was later shown [74] to be due to the slow approach to equilibrium of the gas mixtures.

Unfortunately, the benefit of an MnS layer is not fully realised because FeS dissolves in it extensively, and increases somewhat the deviation from stoichiometry [22,74]. This permits the passage of iron through the MnS, allowing growth of an outer $Fe_{1-\delta}S$ layer. Even so, the benefit conferred by manganese additions is generally superior to that of chromium (Table 8.4). When Fe-Mn alloys are reacted in gases with p_{S_2} below the $Fe/Fe_{1-\delta}S$ equilibrium, they grow external scales and internal precipitates of MnS. Papaiacovou et al. [76] demonstrated that both processes are controlled by alloy diffusion at 700–800°C, but by scale diffusion at 900°C.

TABLE 8.4 Sulphidation Rate Constants, k_w ($g^2\ cm^{-4}\ s^{-1} \times 10^8$), in Following H_2/H_2S [76]

T (°C)	700		800	
p_{S_2} (atm)	10^{-8}	8×10^{-5}	10^{-8}	8×10^{-5}
Fe	4.2	19	8.3	50
Fe-25Cr	2.2	1.6	12	26
Fe-25Mn	0.5	4.4	1.2	9
Fe-25Mn-10Cr	2.5	1.7	6.3	26

Attempts have been made to improve the sulphidation of iron by alloying with both manganese and chromium [75,77]. The ternary alloys provide better performance than Fe-Mn only if both (Mn,Fe)S and $(Cr,Mn)_3S_4$ layers are developed. The observed sequence of scale layers illustrates some of the complexities of these sulphide systems: Fe(Mn)S, Mn(Fe)S, Cr_3S_4 (when present) and Cr(Fe)S from the scale exterior to the alloy surface. This arrangement is consistent with the relative stabilities of the pure sulphides except for the location of MnS (Table 8.1). The explanation lies in the destabilisation of MnS by its approximately 0.5 mol fraction FeS content [75].

An Fe-Mn-Al alloy was found [78,79] to sulphidise more slowly than Fe-Mn alloys at 700°C in H_2/H_2S atmospheres. In the early stages of reaction, manganese depletion from the alloy allowed formation of an aluminium-rich sulphide at its surface. However, this layer does not provide long-term protection: an $Fe_{1-\delta}S$ layer grows above it and the mixed hexagonal sulphide MAl_2S_4 develops beneath it.

8.3.5 Alloying With Molybdenum

The recognition that conventional alloy additions failed to provide sulphidation resistance led some years ago to a series of investigations into the effectiveness of refractory metals as alloy additives. The effects of molybdenum additions to both iron and nickel have been examined. The problem with all of these alloys is illustrated by the inert marker experiment shown in Fig. 8.7. A molybdenum sulphide layer does indeed grow by inward sulphur transport, but an iron or nickel sulphide grows on the outside by outward cation transport. The inner layer has been reported [80,81] to be a mixture of FeS and MoS_2 at high p_{S_2}, and the Chevrel phase $Fe_xMo_6S_{8-z}$ at lower p_{S_2} values. The phase diagram in Fig. 8.8 illustrates the diffusion paths involved. Similar results were found for Ni-Mo alloys [83,84].

Clearly, the alloy-base metal is able to penetrate the molybdenum-rich sulphide phases rather readily, allowing continued reaction. In the case of nickel-base alloys, this can lead to liquid sulphide formation. The permeability of MoS_2 to transition metals is related to its layered structure. Foreign cations can intercalate between adjacent sulphide planes, occupying some of the octahedral sites and, presumably, diffusing via these positions. The more reactive iron species forms the ternary Chevrel phase $Fe_xMo_6S_{8-z}$, in which $1.15 < x \leq 1.35$ and $7.70 < 8 - z \leq 7.90$ at 1000°C [85]. The simultaneous disorder in the iron and sulphide sublattices explains the ability of this compound to diffuse both species.

The performance of Fe-Mo and Ni-Mo alloys can be improved by the addition of aluminium. Douglass et al. [86,87] attributed the enhanced resistance to formation of the double sulphide $Al_xMo_2S_4$ as part of the inner scale layer when $p_{S_2} = 0.01$ atm. Chen et al. [88] found Al_2O_3 and $FeAl_2O_4$ to be formed on Fe-Mo-Al by oxygen present as impurity H_2O in their H_2/H_2S mixtures. He and Douglass [89] arrived at a similar conclusion for Ni-Mo-Al

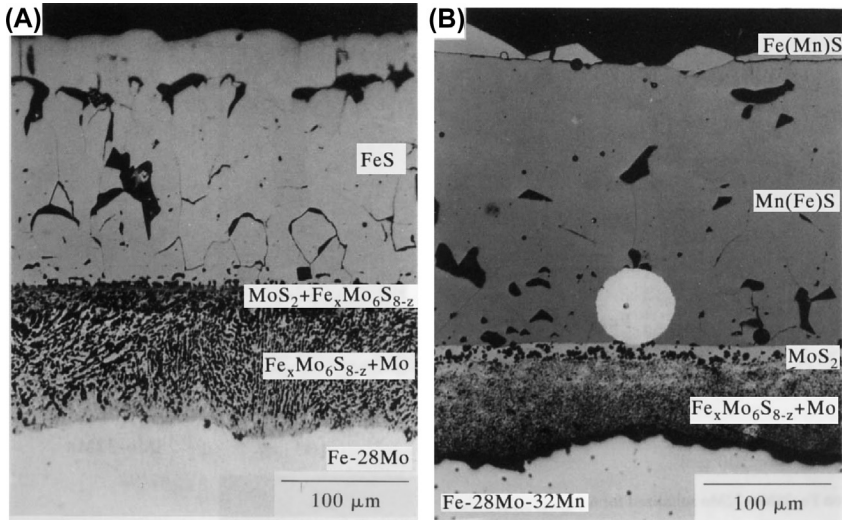

FIGURE 8.7 Sulphide scales grown (A) at 750°C on Fe-27 a/o Mo and (B) at 700°C on Fe-28 Mo-32Mn exposed to H_2/H_2S (showing a Pt marker). *Reprinted from Y. Chen, D.J. Young, S. Blairs, Corros. Sci. 36 (1994) 401, with permission from Elsevier.*

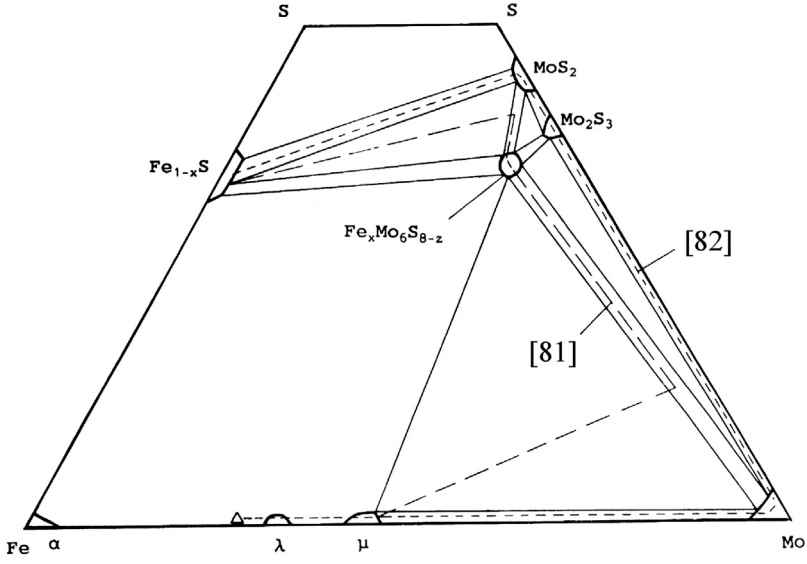

FIGURE 8.8 Fe-Mo-S isothermal section at 750°C [82] showing diffusion paths for FeS layer growth over Mo-rich sulphide. *Reprinted from Y. Chen, D.J. Young, S. Blairs, Corros. Sci. 36 (1994) 401, with permission from Elsevier.*

alloys reacted in H_2/H_2S gases. The addition of manganese [80] and manganese plus aluminium [90] to Fe-Mo alloys enhances their sulphidation resistance. The manganese effect is due to formation of an intermediate Mn(Fe)S layer which slows the growth of an outermost $Fe_{1-\delta}S$ layer, and the aluminium effect is as described above.

8.3.6 Refractory Metal Alloys

The use of niobium as an alloying additive has been examined in detail by Douglass, Gesmundo and co-workers [87,91–94]. Niobium reduces the rate of iron sulphidation only slightly but has a strong effect on nickel sulphidation at subliquidus temperatures (Fig. 8.8) during exposure to 0.01 atm of S_2(g). At temperatures above 635°C, niobium levels of some 30 wt% are required to suppress Ni-S liquid phase formation. The addition of aluminium to Fe-Nb alloys depresses sulphidation rates dramatically (Fig. 8.9). In all cases, the scales consisted of outer layers of either $Fe_{1-\delta}S$ or $Ni_{1-\delta}S/Ni_3S_2$ over an inner, heterogeneous, niobium-rich layer. Platinum markers were invariably found at the interface between the two layers, corresponding to the expected inward sulphur transport through niobium sulphide and outward metal transport through iron and nickel sulphides.

The reduction in rate achieved by niobium alloying is caused by a slowing of iron and nickel diffusion by the inner sulphide layer. This layer was quite

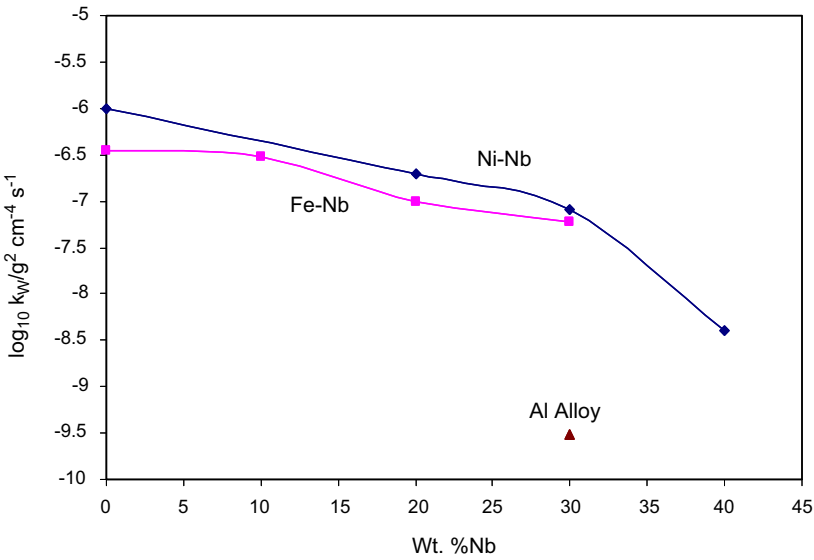

FIGURE 8.9 Effect of Nb concentration on sulphidation in 0.01 atm S_2 of Fe-Nb and Ni-Nb and Fe-30Nb-3Al. *Data points taken from G. Wang, D.L. Douglass, F. Gesmundo, Oxid. Met. 35 (1991) 349; M.F. Chen, D.L. Douglass, F. Gesmundo, Oxid. Met. 31 (1989) 237; G. Wang, R. Carter, D.L. Douglass, Oxid. Met. 32 (1989) 273.*

complex, consisting in the case of Fe-Nb alloys of $Fe_{1-\delta}S$, $FeNb_2S_4$, NbS_2 and particles of intermetallic Fe_2Nb. Intercalation of iron into the layered NbS_2 structure and the coexistence of iron-rich sulphides in the inner layer are thought to explain the disappointing performance of these alloys. Ternary Fe-Nb-Al alloys developed similar scales, with aluminium concentrated in the inner layer. The phase constitution of these layers was not established, and a lack of knowledge of the sulphide properties hampers discussion. It is clear, however, that the presence of aluminium affects both iron and sulphur transport, as both layers grew much more slowly.

The inner layer developed on Ni-Nb alloys consists of $NiNb_3S_6$ plus NbS_2. Nickel diffuses through this layer, but nickel sulphide growth is slowed considerably. Thus although the alloys are unable to form a continuous, protective NbS_2 layer as a result of ternary compound formation, the diffusional blocking effect of the NbS_2 particles and the presumably low value of D_{Ni} in the mixed sulphide lead to a degree of protection. Similar benefits have been obtained for Co-Nb alloys [93,94].

Some limited information is available for titanium sulphide scaling as a result of an interesting application. Because TiO_2 and Al_2O_3 are of comparable stability, the intermetallic TiAl provides marginal resistance to rapid TiO_2 growth. However, titanium sulphides are more stable than Al_2O_3. Selective sulphidation of titanium has been used by Narita et al. [95–97] to form aluminium-enriched alloy surface regions on γ-TiAl in order to improve its subsequent oxidation resistance. Reaction at 900°C in H_2/H_2S gas corresponding to $p_{S_2} = 1.3 \times 10^{-5}$ atm leads to growth of multilayer scales enriched in titanium. The inner layers consist mainly of TiS and Ti_3S_4. However, these layers also contain some aluminium, which diffuses outwards to form a mixed layer of Al_2S_3 and titanium sulphide in roughly equimolar proportions. Sulphidation rates were low.

It is recognised from the foregoing that very high alloying levels of Mo, Al, Nb and/or Mn are required to achieve any benefit in protecting iron and nickel-base materials against high sulphur potentials. No practical alloys have been found. However, coatings based on refractory metals and aluminium may prove to be of use in high sulphur potential environments [98,99]. It should also be observed that the very high sulphur potentials (0.01–1 atm) used in much of the research on refractory metal alloys are seldom encountered in practice. Of more relevance to petroleum and coal conversion processes are H_2/H_2S atmospheres, which are now considered.

8.4 SULPHIDATION IN H_2/H_2S

Low sulphur potentials result from the equilibrium

$$H_2S = H_2 + \frac{1}{2}S_2 \qquad [8.4]$$

for which the standard free energy charge is given in Table 2.1. Mixtures of H_2 and H_2S have often been used in laboratory reactors to control p_{S_2} values.

There is a potential difficulty with this technique at low temperatures, because the rate of H_2S dissociation is slow. Darwent and Roberts [100] showed that the homogeneous gas-phase reaction is bimolecular

$$2H_2S = S_2 + 2H_2 \qquad [8.5]$$

with a rate constant, expressed in $cm^3\ mol^{-1}\ min^{-1}$, of

$$k = 2.27 \times 10^{14} \exp\left(-217\ kJ\ mol^{-1}/RT\right) \qquad [8.6]$$

If the furnace tube through which the gas mixture passes is modelled as a plug flow reactor [101], then the fractional conversion, y, of H_2S to S_2 is given for second order kinetics as

$$\frac{1-y}{y} = \frac{V_T}{k[H_2S]^{\circ}\tau} \qquad [8.7]$$

where V_T is the total volumetric flow rate, τ is the gas residence time and $[H_2S]^{o}$ is the initial, or inlet, concentration. The maximum value of p_{S_2} achievable may therefore be calculated. Results for H_2-H_2S-N_2 mixtures in a typical tubular laboratory reactor are shown in Table 8.5. As expected from Eqs [8.6] and [8.7], H_2S dissociation becomes slower at lower temperatures and greater gas dilution. The actual levels of p_{S_2} reached in the gas can be

TABLE 8.5 Maximum p_{S_2} Values Achieved by H_2S Dissociation[a] in Tubular Flow Reactor Compared With Equilibrium [102]

T (°C)	p_{H_2S} (atm)	p_{S_2}(eq) (atm)	p_{S_2}(max) (atm)
800	1.11×10^{-1}	6.5×10^{-6}	6.5×10^{-6}
	2.4×10^{-2}	6.5×10^{-6}	9.9×10^{-7}
665	3.85×10^{-1}	6.5×10^{-6}	6.5×10^{-6}
	1.43×10^{-2}	6.5×10^{-6}	6.5×10^{-6}
	1.43×10^{-2}	3.3×10^{-9}	3.3×10^{-9}
	5.7×10^{-3}	3.3×10^{-9}	2.4×10^{-9}
520	8.0×10^{-1}	6.5×10^{-6}	1.6×10^{-6}
	6.0×10^{-1}		2.8×10^{-7}
	4.0×10^{-1}		1.3×10^{-7}
	5.0×10^{-2}		7.9×10^{-10}

[a] *Calculated for H_2-H_2S-N_2 mixtures at $P_T = 1$ atm, linear flow rate ≈ 2 cm s^{-1}.*

very low. A simple mass balance calculation shows that the rate at which $S_2(g)$ is regenerated within the gas is too slow to keep up with observed sulphur uptake rates on many metals. Obviously, the reactant species under these conditions is H_2S.

In view of the fact that parabolic scaling is often observed and that Wagner's scaling theory applies, at least in the case of iron sulphidation, it must be supposed that H_2S dissociation occurs on the scale surface. The gas adsorption and dissociation model of Section 2.9 has been applied to the case of iron sulphidation [102], leading to the prediction that the adsorbed layer approaches equilibrium at a rate which increases with p_{H_2S} and decreases with $p_{S_2}(eq)$. These predictions were successful in describing nonsteady-state sulphidation of both iron and Fe-Mn [75].

Data on the sulphidation of iron in H_2S-bearing gases illustrate the importance of recognising this effect. Workers using high temperatures, low diluent concentrations and low values of $p_{S_2}(eq)$ establish a steady-state relatively quickly and commonly report parabolic kinetics [16,17]. Conversely, investigators using significant gas dilutions or low temperatures report nonsteady-state behaviour [70,102–106]. Short reaction times can fail to reveal that the sulphidation rate is increasing and result in underestimates of scaling rates.

Reaction in dilute H_2/H_2S gases can lead to whisker formation. An Fe-Ni alloy is seen in Fig. 8.10 to have developed multiple reaction zones: an inner, compact monosulphide which was overgrown by needles of pentlandite,

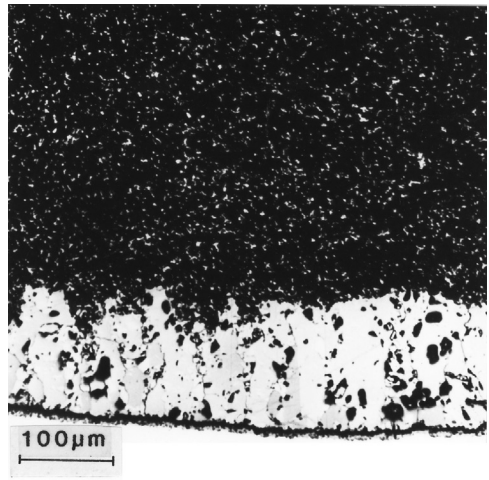

FIGURE 8.10 Cross-section of reaction product layers formed on Fe-41Ni at 520°C, $p_{S_2} = 1.2 \times 10^{-9}$ atm, $p_{H_2S} = 5 \times 10^{-2}$ atm.

$(Ni,Fe)_9S_8$, which were covered in turn by whiskers of Ni_7S_6, covered finally by whiskers of NiS. Measured compositions are shown plotted on the Fe-Ni-S phase diagram in Fig. 8.11, where local equilibrium is seen to be in effect. Consistent with local equilibrium, the kinetics of whisker growth were parabolic [107,108]. The observation that the whiskers were apparently at local equilibrium is at first sight remarkable. The volume fraction of solid in the whisker zone was about 0.05. Although the whiskers were much more numerous and densely arrayed than is usual for corrosion products [109], the whisker zone was clearly permeable to gas.

Despite the openness of the whisker zone, the effective sulphur activity near the base of the whiskers was much less that at their tips. In the example of Fig. 8.11, the whisker tips are NiS, the mid-zone of the whisker layer is Ni_7S_6 and the whisker bases are pentandite. No such sulphur activity gradient could possibly exist if the gas phase were functioning as a sulphur transport medium. The explanation, of course, is that the H_2S dissociation reaction does not reach equilibrium in the gas phase. The phase constitutions of the whisker zones are understandable if the whisker tips, but not their sides, are catalytically active to H_2S dissociation. In this way, the effective sulphur activity is brought close to the equilibrium value at the whisker tip, and the local phase constitution is thereby determined. However, the sulphur activity along the whisker length is controlled by the outward flux of nickel along the whisker. At higher p_{H_2S} and p_{S_2} values, no whiskers develop, and a compact nickel-rich outer sulphide layer grows instead.

A final complication which sometimes arises in these gases is the dissolution of hydrogen into the sulphide. The effect is unimportant in the widely

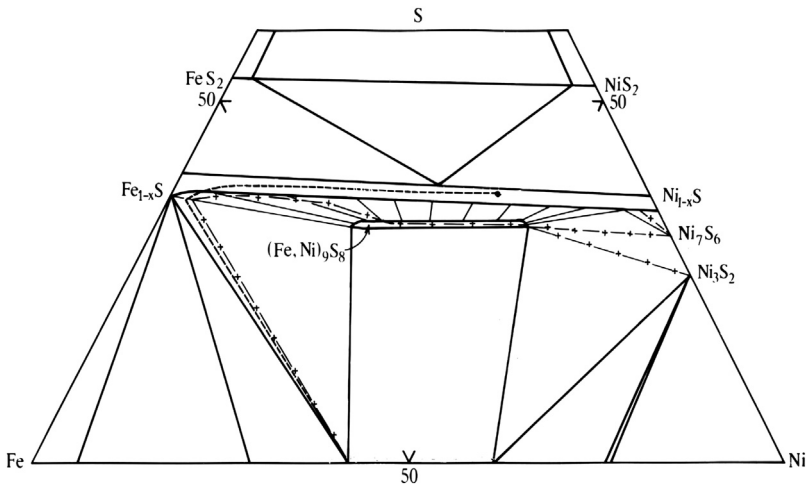

FIGURE 8.11 Isothermal section of Fe-Ni-S phase diagram at 520°C showing diffusion path for Fig. 8.10.

nonstoichiometric NiAs-type sulphides, but it has been shown to accelerate the sulphidation of molybdenum at high temperatures [29,110]. The variation in k_p with hydrogen partial pressure at fixed p_{S_2} values can be rationalised in terms of hydride doping.

8.5 EFFECTS OF TEMPERATURE AND SULPHUR PARTIAL PRESSURE

Sulphide electronic conductivities are usually metallic in nature, and Wagner's rate Eq. [3.61] can be written

$$k_p = \int_{a'_S}^{a''_S} D_M \frac{1}{1-\delta} d \ln a_S \qquad [8.8]$$

for growth of an $M_{1-\delta}S$ scale. This rate constant varies with temperature through the thermal activation of D_M, the temperature effect on the scale-alloy local equilibrium (which sets the integration limit a'_S) and the temperature effect on the functional relationship between δ and a_s. The last effect is important if the degree of intrinsic disorder, and hence nonstoichiometry, is large (Eqs [3.15] and [3.19]). This is the case for the NiAs-type sulphides, which are the most frequently encountered in practice. A proper accounting for the effect requires numerical integration (Section 3.7), but it is usually ignored because insufficient data are available.

The data in Table 8.2 show that apparent activation energies for growth of the NiAs-type sulphides differ considerably with p_{S_2}. These sulphides contain cation defects, predominantly metal vacancies in the monosulphides. If scale growth is controlled by cation vacancy diffusion, then Wagner's theory leads to Eq. [3.84], rewritten here as

$$k_p = k_o p_{S_2}^{1/n} \qquad [8.9]$$

with $n = 2(m + 1)$ and m as the effective vacancy charge. The limited data in Table 8.2 are consistent with doubly charged vacancies in $Fe_{1-\delta}S$ and MnS, and close-to-neutral vacancies in $Co_{1-\delta}S$.

The apparent variation of activation energy with p_{S_2} is therefore understandable from Eq. [8.8]. At low p_{S_2} values, $\delta \ll 1$, and according to Eq. [8.8], k_p is approximately independent of δ and its temperature effect. At high p_{S_2} values, δ becomes large and its temperature dependence affects k_p. This argument succeeds for $Fe_{1-\delta}S$ but is inapplicable to cobalt which grows a multilayer scale. The different E_A values reported for manganese sulphidation cannot be rationalised in this way, as $\delta \ll 1$ at all p_{S_2} values. Inconsistent E_A values have been reported for chromium sulphidation in 1 atm S_2(g).

As some refractory metal sulphides grow by diffusion of sulphur, a different dependence of rate on p_{S_2} is expected. According to Wagner's theory, an expression like Eq. [3.90] will apply:

$$k_p = \left[k_o\left(p'_{S_2}\right)^{-\frac{1}{n}} - \left(p''_{S_2}\right)^{-\frac{1}{n}}\right] \qquad [8.10]$$

Since p'_{S_2} is small, the rate is almost independent of the ambient p_{S_2} if the latter is at high levels. This reflects the fact that sulphur vacancies are injected at the metal-sulphide interface, and their concentration at this location is unaffected by gas-phase conditions. However, as p''_{S_2} is lowered to approach p'_{S_2}, alterations in its value will change the sulphur activity gradient and hence, k_p. Study of this effect is complicated in the case of molybdenum, which sulphidises in H_2/H_2S at faster rates than in S_2(g) at the same p_{S_2} value [29,111], as a result of hydrogen dissolution in the sulphide. Experiments in H_2-H_2S-N_2 gas mixtures allowed investigation of the effect of variation in p_{H_2} while p_{S_2} was maintained constant. Results showed that k_p increased with p_{H_2}, consistent with hydride dissolution [111].

The behaviour of $Nb_{1+\delta}S_2$ is interesting. Gesmundo et al. [43,112] showed that pure niobium sulphidised in H_2/H_2S at rates which increased with p_{S_2}. This was interpreted in terms of cation diffusion. However, this mode of transport is not reflected in the sulphidation of M-Nb alloys (M = Fe, Ni or Co), which form duplex scales with an inner, niobium rich layer which grows by inward sulphur diffusion. A direct comparison is not possible, because the alloy-scale layers are multiphase, containing other phases which might be responsible for the sulphur transport.

8.6 THE ROLE OF OXYGEN

As noted earlier, reaction in H_2/H_2S mixtures invariably involves impurity amounts of H_2O. Although the levels are very low, they can be sufficient to oxidise aluminium. Under these conditions, it is possible that the Al_2O_3 contributes substantially to protection against sulphur attack. This question has been investigated using controlled $H_2/H_2O/H_2S$ gas mixtures for a number of alloys.

Iron-aluminium-based alloys containing various additions of titanium and/or chromium were found by Regina et al. [113] to be protected at 500°C by a thin Al_2O_3 scale when exposed to $H_2/H_2O/H_2S$ mixtures. Various workers [114–117] have shown that preoxidation of FeCrAl alloys provides them with a degree of protection against subsequent exposure to mixed oxidising – sulphidising gases. The performance improves with extent of preoxidation.

Douglass et al. [118,119] showed that the addition of 7 wt% aluminium to Fe-20Mo and Fe-30Mo was sufficient to form Al_2O_3 at 700–980°C in $H_2/H_2S/H_2O$ atmospheres corresponding to $p_{S_2} \sim 10^{-5}$ atm and $p_{O_2} \sim 10^{-20}$ atm. With 9–10 wt% Al, exclusively Al_2O_3 scales were formed, sulphidation

being completely prevented. Qualitatively similar benefits were achieved with Ni-Mo-Al alloys in $H_2/H_2S/H_2$ gases [120]. The results were complicated by the formation of the double sulphide $Al_{0.55}Mo_2S_4$.

It is clear from the work on aluminium-containing alloys that Al_2O_3 formation provides the best possibility of protection against sulphur corrosion. However, formation of the necessary continuous alumina layer requires a sufficiently high interfacial aluminium concentration, $N_{Al,i}$. As seen from Eq. [6.11], this requires both high alloy levels of aluminium and high diffusivities. At the relatively low temperatures involved in some sulphur corrosion processes, D_{Al} will be low and the value of $N_{Al}^{(o)}$ required makes austenitic alloys impractical. Recognition of this problem has led to numerous investigations into the performance of metal aluminides. Iron aluminides have been shown by Tortorelli et al. [121–123] to have particularly good resistance to sulphidation as a result of their ability to develop protective Al_2O_3 layers. An Fe-40 wt% Al alloy was found by Lang et al. [124] to exhibit excellent resistance to H_2/H_2S gases containing up to 9.7 v/o H_2S at 900 and 1000°C. Again, protection was due to Al_2O_3 formation.

Nickel aluminides are much less successful, as a result of rapid nickel sulphide growth when the sulphur potential is high enough to stabilise these reaction products. Natesan [67] showed that the γ'-Ni_3Al intermetallic failed by sulphidation in this way at 875°C, being unable to form Al_2O_3. Schramm and Auer [125] demonstrated the same result for Ni-Al binaries containing 25–45 wt% Al exposed to $H_2/H_2O/H_2S$ at 750–950°C. The β-NiAl intermetallic also fails to develop a protective Al_2O_3 scale [68,126].

The performance of several chromia- and alumina-forming alloys and coatings in the reducing, sulphidising conditions expected of coal gasification have been explored, and the interested reader is referred to Refs [127–130].

8.7 INTERNAL SULPHIDATION

Internal sulphidation is seldom studied, as the rate at which an alloy is consumed by scaling often exceeds the rate at which sulphur can diffuse into the alloy. Under these conditions, the rapidly receding scale-alloy interface sweeps up and incorporates any internal precipitates. However, if the reaction is carried out at such a low p_{S_2} value that no external sulphide scale forms, or if a slowly growing oxide scale is penetrated by sulphur, internal sulphidation can result. Studies on model systems might provide information on sulphur permeabilities for use in predicting corrosion rates for more practical materials. Unfortunately, there are practical problems with this approach.

In the first place, because sulphide stabilities are relatively low, their solubility products in iron and nickel-base alloys are high (see Eqs [2.82]–[2.90]). Consequently, the simple Wagner description of internal sulphidation kinetics leads to quantitative error. Secondly, thermodynamic interactions between solute metals and dissolved sulphur can be rather large. Finally, it has been

clearly established [131–133] that sulphur diffuses preferentially along alloy grain boundaries over a wide range of temperatures, leading to intergranular sulphide precipitation.

Austenitic heat-resisting steels have been found [129,134–136] to undergo intergranular sulphidation during exposure to mixed oxidising-sulphidising gases, and in reaction with pure $S_2(g)$. Unfortunately, it is currently not possible to predict how the rate of this process will change with alloy composition or temperature.

8.8 HOT CORROSION

The combustion of fossil fuels and the incineration of waste often produces condensed phases as well as combustion gas. Ash is generated from mineral components of the burning materials and can be expected to deposit on equipment surfaces. In addition, sulphur impurities are burnt to form SO_3, which reacts with alkali metals to form stable sulphates. Small amounts of salt in the air are sufficient to promote reactions such as

$$SO_3 + H_2O + 2NaCl = Na_2SO_4 + 2HCl \qquad [8.11]$$

Pure Na_2SO_4 has a melting point of 884°C and can condense as a liquid on hardware exposed to the gases. (The presence of other solutes in the sulphate will change this melting point.) Liquid sulphates are ionic melts. Interactions between them and metals are therefore electrochemical in nature, involving oxidation of the metal in an anodic process such as

$$M = M^{n+} + ne^- \qquad [8.12]$$

and reaction of salt species [137,138]

$$S_2O_7^{=} + e^- = SO_4^{=} + SO_3^- \qquad [8.13]$$

$$SO_3^- + e^- = SO_2 + O^{=} \qquad [8.14]$$

supported by the dissolution reaction

$$SO_3 + SO_4^{=} = S_2O_7^{=} \qquad [8.15]$$

This process is clearly analogous to the electrochemical corrosion of metal in aerated water, in which the dissolved oxygen is reduced to hydroxide. As we will see, there is a further analogy in that hot corrosion is a dissolution-reprecipitation process, like the rusting of iron, in which the step Eq. [8.12] is followed by solid compound formation.

Other liquid phases can be produced in combustion processes. Fuel oils can contain small amounts of vanadium which forms a series of oxides, up to V_2O_5 with a melting point of 690°C. Various sodium vanadates can form, with melting points around 550–700°C. The combustion of biomass together with coal can generate large amounts of Na_2SO_4 and/or K_2SO_4. Finally, waste

incineration produces chemically diverse condensed phases, principally sulphates and chlorides. All of these liquid phases cause accelerated attack, or 'hot corrosion'. Attention will be restricted in this chapter to sulphate-induced hot corrosion. Several other molten salt-induced corrosion processes are discussed in Chapter 12, and the reader is referred to reviews by Paul and Seeley [140] and Rocca et al. [141] for an account of vanadium-induced hot corrosion.

8.8.1 Phenomenology of Sulphate-Induced Hot Corrosion

The subject has been reviewed by Stringer [139,142], Pettit and Giggins [143], Kofstad [144] and Rapp [145,146]. The principal application is the accelerated corrosion of gas turbine hot stage components, a field which continues to be a focus for research. Hot corrosion in gas turbines is caused by salt deposition in the engines, a subject which has been reviewed by Bornstein and Allen [147]. The resulting damage can be severe, as seen from the example of hot corrosion damage to a diffusion coating, shown in Fig. 8.12.

When sulphate-induced hot corrosion was first investigated, it was thought [148,149] that alloy sulphidation by the salt was a necessary precursor to accelerated attack. In a series of key papers, Bornstein and De Crescente [150–152] and Goebel and Pettit [153] established the essential elements of the hot corrosion phenomenon. The role of sulphur was shown to be nonessential by the finding that oxidation of presulphidised superalloys did not lead to accelerated corrosion. Furthermore, exposure to molten Na_2CO_3 or Na_2NO_3 did cause accelerated reaction, just like Na_2SO_4. Bornstein and De Crescente proposed that the alloy's protective oxide scale was attacked by Na_2O, the

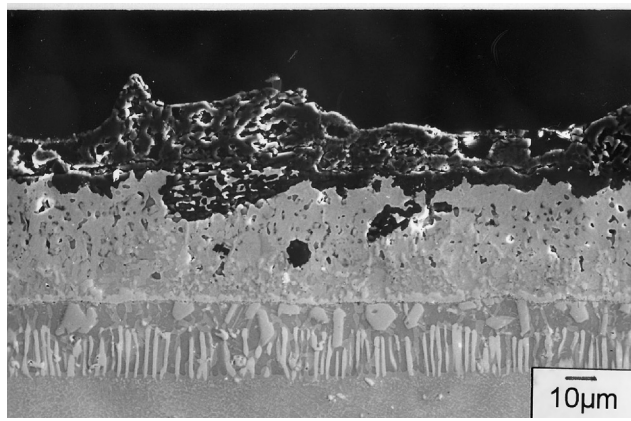

FIGURE 8.12 SEM view of damage to a model chromium-modified nickel aluminide coating on a René 80H nickel-base superalloy after 18 h exposure at 900°C to a molten Na_2SO_4 film in a gas of O_2-1% SO_2. Porous oxide has developed along with internal sulphidation.

basic component of all three molten salts used. Goebel and Pettit also interpreted hot corrosion of nickel in the same way, ie, dissolution of NiO into a basic melt, and added the additional step of NiO reprecipitation at other locations.

This mechanism explained the experimentally observed induction period prior to rapid reaction. It corresponds to the time taken for dissolution of the protective oxide to occur, allowing direct access of the melt to the underlying alloy. The model was extended by Goebel et al. [154] to describe hot corrosion of alloys containing acidic oxide formers such as vanadium or molybdenum. As is discussed below, the metal oxides of interest are soluble also in acidic melts. In order to evaluate oxide solubilities, it is necessary first to consider the thermodynamics and electrochemistry of the melt.

8.8.2 Molten Salt Chemistry

The thermodynamics of oxyanion melts are conveniently described in terms of equilibrium with the oxide anion and the appropriate gas species. Thus, for a sulphate melt

$$SO_4^{=} = O^{=} + SO_3(g) \qquad [8.16]$$

and corresponding equilibria can be written for carbonates and nitrates. In the hot corrosion literature, the reaction (Eq. [8.16]) is conventionally written as

$$Na_2SO_4 = Na_2O + SO_3(g) \qquad [8.17]$$

from which it follows that

$$\log a_{Na_2O} + \log p_{SO_3} = -\Delta G_{17}^{\circ}/2.303\ RT \qquad [8.18]$$

The equilibrium is described as an acid-base reaction, with Na_2O (or $O^{=}$) the base and SO_3 the acid. At a fixed temperature, the thermodynamic state of a sodium sulphate melt is then specified by the values of the oxygen potential plus the melt basicity, defined as $-\log a_{Na_2O}$ by analogy with the pOH of aqueous solutions.

The various possible states for the Na-S-O system are shown in the phase diagram of Fig. 8.13. The melt stability regime is seen to be large, implying that a film of this liquid on a metal surface can sustain large gradients in oxygen potential and basicity. The diagram can be calculated from standard free energy data, using the methods of Section 2.2 [155]. The assumption of unit activity for condensed phases is used to define the phase boundaries in the diagram. The sulphate melt phase field is shown subdivided into regions corresponding to different predominant ionic minority species. The local chemical state in any melt can be determined electrochemically [145,146], using a ZrO_2 electrode to measure oxygen activity and a sodium-conducting solid electrolyte to measure a_{Na}.

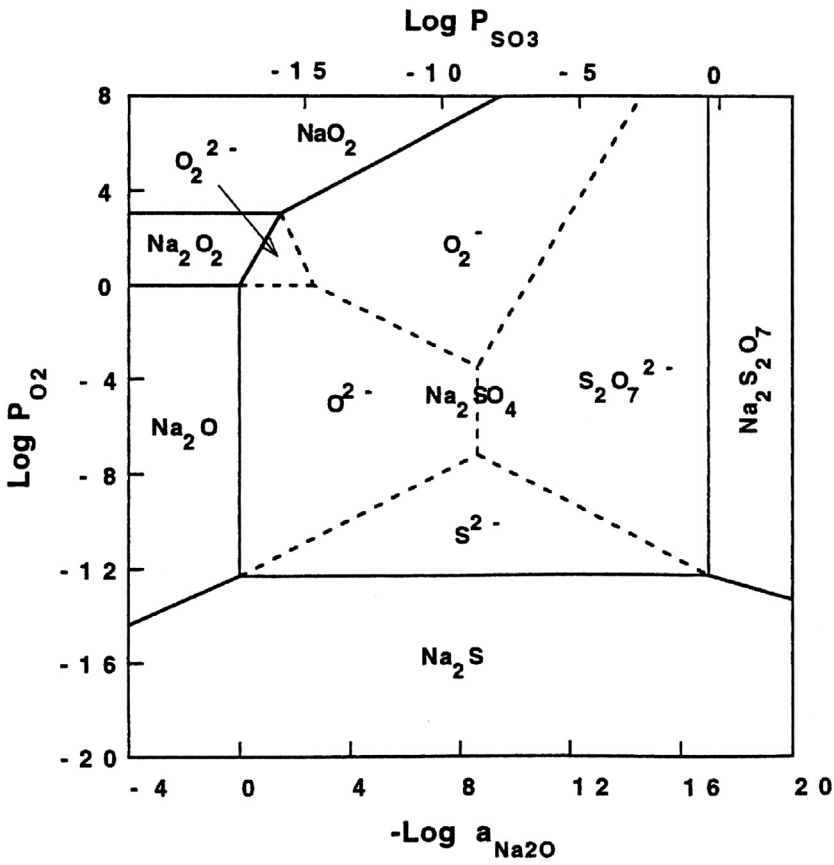

FIGURE 8.13 The Na-S-O phase diagram for 900°C [155]. *Reproduced by permission of The Electrochemical Society.*

The next step is to superimpose the Na-S-O phase diagram on the corresponding one for the corroding metal, following the procedure of Quets and Dresher [156]. The example of nickel is shown in Fig. 8.14. As can be seen, nickel metal is stable in contact with the melt in only a very small region. Similar diagrams for iron, chromium and aluminium show that these metals have no regions of stable coexistence with molten Na_2SO_4. The development of new phases and the extent of their intersolubility must therefore be investigated.

Nickel forms a solid sulphate (Fig. 8.14), but only at very high p_{SO_3} values. However, $NiSO_4$ dissolves readily in Na_2SO_4 [157]. Its activity as a melt solute is represented by the dotted lines in the figure. In addition, Gupta and Rapp [158] concluded (see below) that the NiO_2^- anion forms, and its isoactivity lines are also shown in Fig. 8.14. Rapp and co-workers [158–162],

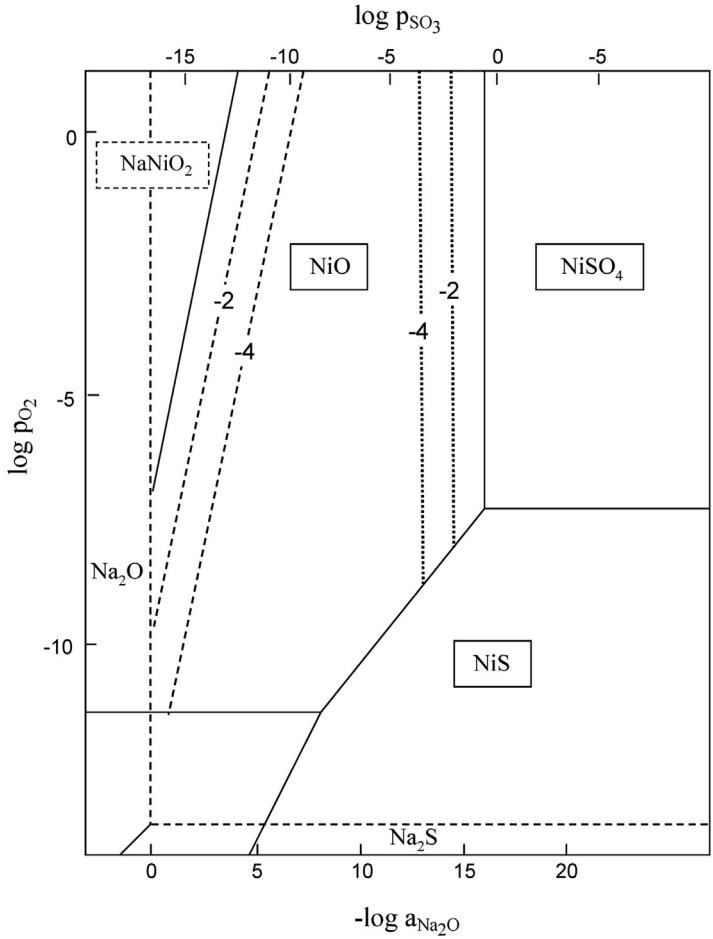

FIGURE 8.14 Phase stability diagram for Ni-S-O at 900°C in the presence of Na_2SO_4.

Deanhardt and Stern [163] and Misra et al. [164], measured oxide solubilities in Na_2SO_4 melts. Data for $p_{O_2} = 1$ atm and $T = 927°C$ are summarised in Fig. 8.15. Most oxides are seen to exhibit two regimes of dissolution separated by a minimum behaviour which can be understood in terms of basic and acidic dissolution.

Consider the example of NiO dissolution via basic dissolution

$$2NiO + \frac{1}{2}O_2(g) + O^{2-} = 2NiO_2^{=} \qquad [8.19]$$

and acidic dissolution

$$NiO = Ni^{++} + O^{=} \qquad [8.20]$$

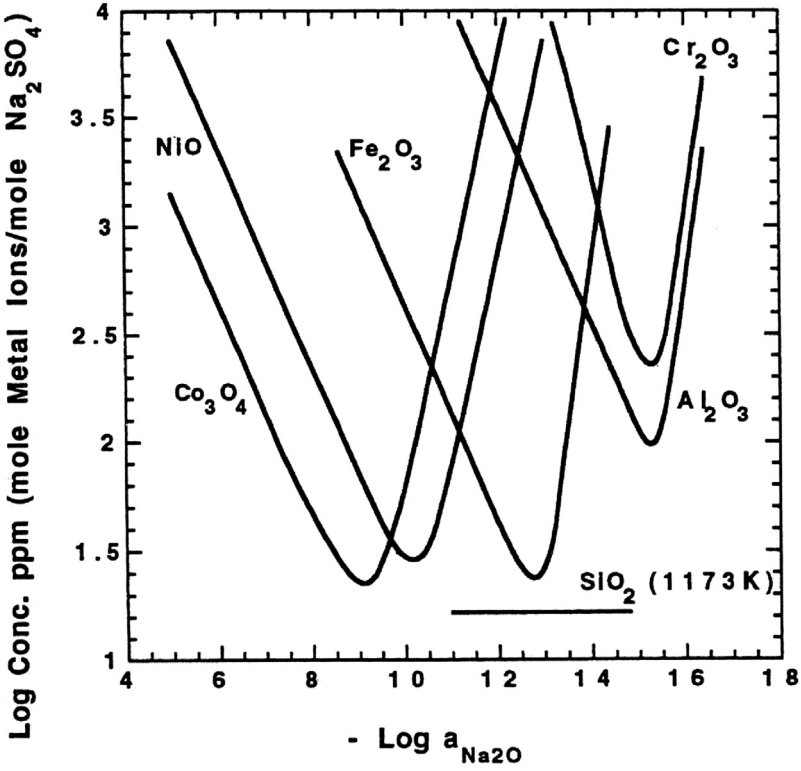

FIGURE 8.15 Measured oxide solubilities in molten Na_2SO_4 at 927°C and oxygen pressure of 1 atm [146]. *With kind permission from Springer Science and Business Media.*

The corresponding equilibrium expressions are used to derive the dependence of nickel solute activity on basicity:

$$\left.\frac{\partial \log a_{NiO_2^=}}{-\partial \log a_{Na_2O}}\right|_{p_{O_2}} = -\frac{1}{2} \qquad [8.21]$$

$$\left.\frac{\partial \log a_{Ni^{++}}}{-\partial \log a_{Na_2O}}\right|_{p_{O_2}} = 1 \qquad [8.22]$$

The measured [158] slopes of nickel solute concentration versus $-\log a_{Na_2O}$ were in good agreement with these predictions. Assuming that the dilute solutions were Henrian, it is concluded that the acidic and basic dissolution processes are correctly formulated. The conclusion was reinforced by the finding that the dependence on p_{O_2} of the basic solubility was correctly predicted.

Although it has been shown that the oxides of importance to high-temperature alloys will dissolve in sulphate melts, their solubilities can be rather low (Fig. 8.15). The question therefore arises as to why a hot corrosion reaction does not become very slow, at least in a quiescent melt, as it becomes saturated at the oxide-sulphate interface. The answer lies, of course, in continuing mass transport within the melt.

8.8.3 Fluxing Mechanisms

A flux of solute metal into the salt deposits will be maintained if an appropriate activity gradient exists. Rapp and Goto [165] pointed out that this would be the case if the solubility decreased monotonically with increasing distance into the sulphate film. The mechanism is shown schematically in Fig. 8.16. The greater extent of precipitation arrived at with increasing values of x means that less metal remains in solution, and therefore

$$\frac{\partial C_{M^+}}{\partial x} < 0 \qquad [8.23]$$

A diffusion flux results from this gradient. The required gradient in solubility cannot result from the expected gradient in a_o, as shown in reaction

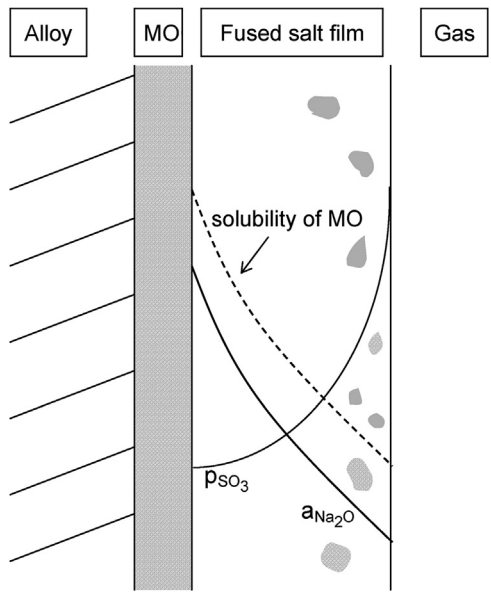

FIGURE 8.16 Hot corrosion by dissolution and reprecipitation in a molten salt film. *Based on model of N. Otsuka, R.A. Rapp, J. Electrochem. Soc. 137 (1990) 46.*

[8.19]. However, variation in salt basicity with position will cause gradients in solubility in both basic and acidic fluxing regimes (Fig. 8.15).

Basic fluxing into molten sulphate stabilised at its outer surface by the presence of gaseous SO_3 is readily understood. Local penetration of the oxide scale by molten salt places the metal in contact with a low a_o and high a_S liquid, leading to its sulphidation. Removal of sulphur from the liquid increases its basicity at the solid-molten salt interface, whereas the continuing presence of SO_3 at the liquid-gas interface maintains a more acidic condition at this boundary. The required gradient in a_{Na_2O}, and therefore in C_{M+}, is thereby achieved. The additional gradient in a_{SO_3} can drive anion diffusion, maintaining a sulphidation reaction. This sequence of steps has been demonstrated in the case of pure nickel by Otsuka and Rapp [166], using electrochemical monitoring to map reaction progression on the phase diagram of Fig. 8.13. The reaction morphology of Fig. 8.12 is also accounted for: sulphide is formed at and beneath the alloy surface, and reprecipitated oxide forms a porous deposit rather than a compact scale.

Acidic fluxing can occur if the melt is more acid at the material-melt interface than at the melt-gas. This can occur during corrosion of alloys, when the dissolution of one component creates the gradient in basicity necessary to flux another [167]. Dissolution of alloy components molybdenum and tungsten produces the strongly acidic oxides MoO_3 and WO_3, and much enhanced oxide stability through their ability to form complexes. A negative gradient in the acidic species is expected to result from its evaporation at the melt-gas interface.

Both fluxing mechanisms account for the observed development of porous oxides via reprecipitation during hot corrosion. Of course, the reactive steady-state implied by the model (Fig. 8.16) is unrealistic. Firstly, the model ignores the effect of metal sulphide formation. As seen earlier in this chapter, these sulphides are rapid diffusers, and their growth is important to the overall process. Moreover, this process consumes sulphur and destabilises the melt unless further SO_3 is supplied from the gas. Secondly, the role of the melt as an inexhaustible supply of fluxing ions to be recycled in the fluxing process can only be fulfilled if its overall chemistry remains unaltered. This requires a constancy of boundary conditions, particularly of p_{SO_3}, seldom achieved in practice. Finally, as the reaction proceeds and more porous oxide accumulates, the melt phase is attenuated, and the maintenance of a continuous liquid diffusion path becomes impossible. Nonetheless, the fluxing mechanisms originally proposed by Bornstein and De Crescente [150–152] and Goebel et al. [153,154] provide useful accounts of hot corrosion. The electrochemical measurements of Rapp et al. [158–162] have demonstrated that virtually all metals of importance to high-temperature alloys are subject to attack by liquid sulphates.

8.8.4 Type I and Type II Hot Corrosion

Two temperature regimes of molten sulphate-induced corrosion are observed for nickel and cobalt and their alloys. At temperatures around 900°C, pure Na_2SO_4 is liquid, and corrosion occurs as described above. This is termed Type I hot corrosion. However, hot corrosion can also occur well below the Na_2SO_4 melting point of 884°C. Rapid attack at temperatures of 650−670°C was found by Luthra and Shores [168] to result from formation of $NiSO_4$ - Na_2SO_4 or $CoSO_4$ - Na_2SO_4 ternary melts. The mechanism was thought to be acidic fluxing and was observed for a series of Co-Cr, Co-Al and Co-Cr-Al alloys [169]. This is Type II hot corrosion. Under these conditions, formation of a passivating Cr_2O_3 or Al_2O_3 layer was found to be difficult. Similar results have been obtained for iron-based alloys, due to the formation of low melting $FeSO_4$ - Na_2SO_4 ternary salts solutions [170,171].

The morphology of Type II hot corrosion is one of nonuniform attack, with pits of different sizes growing into the metal. Measuring the rate is therefore difficult, and lifetime predictions require complex and rather empirical statistical models [172].

The role of chromium and aluminium in providing protection against hot corrosion is seen from Fig. 8.14 to be limited by the relatively high solubilities of their oxides in molten sulphate. Early electrochemical measurements by Rahmel et al. [173,174] on nickel- and cobalt-base superalloys showed that passivation of chromia-forming alloys occurred at intermediate potentials, but not at more anodic potentials where acidic corrosion occurred. Alumina-forming alloys did not form a protective scale at all, but aluminide and platinum-modified aluminide coatings could form protective Al_2O_3. Later studies of superalloy hot corrosion have been numerous and will not be reviewed here. However, they are in general agreement that these alloys contain too little chromium and aluminium to resist hot corrosion. Some representative superalloy compositions are shown in Table 1.2 and Appendix A.

There remain two possible routes to protection against hot corrosion when salt deposition cannot be avoided: operation at temperatures above the salt dew points, or provision of hot corrosion-resistant coatings. The development of conventional metallic coatings has been reviewed by Goward [175], and that of thermal barrier coatings by Clarke and Levy [176]. The metal coatings are very rich in aluminium or contain high levels of both aluminium and chromium (Table 1.2). Thermal barrier coatings are stabilised zirconia. Modifications to metal coatings designed to improve their corrosion resistance by adding chromium or platinum group metals [177−185] continue to be investigated.

8.9 ACHIEVING SULPHIDATION RESISTANCE

As we have seen, most metals of practical importance react with $S_2(g)$ at unacceptably rapid rates. The reasons for this have been made clear by a large body of research: many metal sulphides contain large concentrations of rather mobile point defects, which support rapid diffusion. In addition, low melting point eutectics are formed in a number of metal–metal sulphide systems. Efforts to achieve sulphidation resistance by alloying have centred largely around the use of refractory metals, which form stable, slow-growing sulphides. The resulting alloys do possess superior sulphidation resistance, but they are impractical as engineering materials.

It is recognised, however, that dealing with pure sulphur gas is a most unusual requirement. Sulphidising environments of practical importance usually contain either H_2S or SO_2, depending on the process in question. Solutions to the oxidising–sulphidising problem are discussed in Chapter 4 and involve stable oxide-forming alloys. It is convenient to consider reducing, sulphidising environments according to their temperatures. A good example is provided by the oil refining industry.

Crude oil distillation units operate at temperatures below 300°C, and low alloy steels are sufficient to resist the organic sulphur species encountered. Hydrodesulphurisation is used to remove sulphur from the process stream by converting it to H_2S. Operating temperatures are in the range 300–400°C, and effective sulphur activities are low. Under these conditions, chromium-bearing steels provide adequate protection, producing slow-growing sulphide scales. Subsequent higher-temperature processing can then be carried out without fear of sulphur corrosion.

Avoiding high temperatures is not always possible when handling H_2S. Pyrometallurgical processing of sulphide ores and gasification of coal provide examples where reducing, sulphurising gases must be handled at elevated temperatures. The materials solution in these cases is to use refractory oxide-lined process vessels and gas mains in the high-temperature regions of the plant. A problem arises, however, if there is a need to pass the hot gases through heat exchangers. The thermal efficiency of heat exchangers is generally best when metal surfaces are used, so high-temperature sulphidation resistance will be required.

As we have seen, alloys which form stable oxides provide good resistance to attack by H_2S. Depending on the process, alumina formers may prove adequate in these applications. At still lower oxygen activities, coatings will be required. It is here that the fundamental research on sulphidation-resistant refractory metal alloys is likely to prove of practical value.

Molten sulphate-accelerated corrosion is essentially an electrochemical dissolution-reprecipitation process. One practical way of achieving resistance

to this form of attack involves avoiding the deposition of molten salts. This can be done by ensuring a clean gas, or by controlling the temperature of equipment surfaces so as to prevent liquid condensation. When these approaches are impossible, as for example in a waste incinerator, the materials solution is to use refractory lined equipment. A somewhat similar approach is adopted for gas turbine engines. Metal surfaces are coated with materials which either are oxides or which develop resistant oxides.

REFERENCES

[1] T. Rosenqvist, J.I.S.I. 176 (1954) 37.
[2] P. Hagan, J.F. Elliott, Trans. AIME 239 (1967) 513.
[3] H. Rau, J. Less, Common Met. 55 (1977) 205.
[4] O. Kubaschewski, C.B. Alcock, P.J. Spencer, Materials Thermochemistry, sixth ed., Pergamon, Oxford, 1993.
[5] T.R. Stubbles, F.D. Richardson, Trans. Faraday Soc. 56 (1960) 1460.
[6] O. Kubaschewski, O. Von Goldbeck, Metalloberflache A 8 (1954) 33.
[7] K.N. Strafford, Metal. Mater. 3 (1969) 409.
[8] D.J. Young, Rev. High Temp. Mater. 4 (1980) 229.
[9] S. Mrowec, K. Przybylski, High Temp. Mater. Proc. 6 (1984) 1.
[10] S. Mrowec, Oxid. Met. 44 (1995) 177.
[11] K. Natesan, Corrosion 41 (1985) 646.
[12] S. Mrowec, T. Werber, Chemia Analit. 7 (1962) 605.
[13] T. Narita, K. Nishida, Trans. Jpn. Inst. Met. 14 (1973) 439, 447.
[14] T. Narita, K. Nishida, Proc. 5th Int. Congress Metallic Corros., NACE, Houston, TX, 1974, p. 719.
[15] R.A. Meussner, C.E. Birchenall, Corros. 13 (1957) 677.
[16] E. Fryt, V.S. Bhide, W.W. Smeltzer, J.S. Kirkaldy, J. Electrochem. Soc. 126 (1979) 684.
[17] D.J. Young, W.W. Smeltzer, J. Electrochem. Soc. 123 (1976) 229.
[18] T. Biegun, A. Bruckman, S. Mrowec, Oxid. Met. 12 (1978) 157.
[19] A. Davin, Cobalt 30 (1966) 19.
[20] D.P. Whittle, S.K. Verma, J. Stringer, Oxid. Met. 5 (1972) 169.
[21] F.A. Elrefaie, W.W. Smeltzer, Oxid. Met. 16 (1981) 267.
[22] K. Nishida, T. Narita, T. Tani, G. Sasaki, Oxid. Met. 14 (1980) 65.
[23] K. Ohta, K. Fueki, T. Mukaibo, Denki Kagaku 38 (1970) 822.
[24] L. Czerski, S. Mrowec, T. Werber, J. Electrochem. Soc. 109 (1962) 273.
[25] K. Nishida, K. Nakayama, T. Narita, Corros. Sci. 13 (1973) 759.
[26] S. Mrowec, T. Werber, M. Zastawnik, Corros. Sci. 6 (1966) 47.
[27] M.S. Kovalchenko, W.W. Syczew, D.Z. Jurezenko, I.G. Traczenko, in: Izv. Akad. Nauk SSSR. Metally, 5 (1974) 221.
[28] J. Gerlach, M.J. Hamel, Metall 23 (1969) 1006, 24 (1970) 488.
[29] B.S. Lee, R.A. Rapp, J. Electrochem. Soc. 131 (1984) 2998.
[30] C.N.R. Rao, K.P.R. Pisharody, Prog. Sol. State Chem. 10 (1975) 207.
[31] W.D. Halstead, Corros. Sci. 15 (1975) 603.
[32] F. Jellinek, Acta Crystallogr. 10 (1957) 620.
[33] L.I. Staffanson, Met. Trans. B 7B (1976) 131.
[34] H. Rau, J. Phys, Chem. Solids 39 (1978) 339.

[35] D.J. Young, W.W. Smeltzer, J.S. Kirkaldy, J. Electrochem. Soc. 120 (1973) 1221.
[36] M. Danielewski, in: 9th Int. Cong. Met. Corros., vol. 4, NRCC, Ottawa, 1984, p. 304.
[37] K. Fueki, J.B. Wagner, J. Electrochem. Soc. 112 (1965) 970.
[38] H. Rau, J. Phys, Chem. Solids 41 (1980) 765.
[39] F. Jellinek, G. Brauer, H. Muller, Nature 185 (1960) 376.
[40] G.A. Wiegers, F. Jellinek, J. Solid State Chem. 1 (1970) 519.
[41] T. Tatsuki, M. Wakihara, M. Taniguchi, J. Less Common Met. 68 (1979) 183.
[42] D. Hodouin, Met. Trans. B 6B (1975) 223.
[43] F. Gesmundo, F. Viani, Y. Niu, Oxid. Met. 38 (1992) 465.
[44] M. Saeki, M. Onoda, J. Less Common Met. 108 (1985) 327.
[45] B. Pei, T. Rosenqvist, Scan. J. Met. 20 (1991) 331.
[46] M.J. Ferrante, J.M. Stuve, H.C. Ko, R.R. Brown, High Temp. Sci. 14 (1981) 91.
[47] S.R. Shatynski, Oxid. Met. 11 (1977) 307.
[48] A. El Goresy, G. Kullerud, in: Meteorite Research, P.M. Millman (Eds.), Reidel Publishing Company, Holland, Dordrecht, 1969, p. 638.
[49] L.V. Mallia, D.J. Young, Oxid. Met. 21 (1984) 103.
[50] S. Mrowec, T. Walec, T. Werber, Oxid. Met. 1 (1969) 93.
[51] K.N. Strafford, R. Manifold, Corros. Sci. 9 (1969) 489.
[52] T. Narita, K. Nishida, Oxid. Met. (6) (1973) 157, 181.
[53] P. Hancock, in: Proc. 1st Int. Conf. Metallic Corrosion, Butterworths, London, 1962, p. 193.
[54] G. Romeo, W.W. Smeltzer, J.S. Kirkaldy, J. Electrochem. Soc. 118 (1971) 1336, 119 (1972) 1267.
[55] J.A. Chitty, W.W. Smeltzer, J. Electrochem. Soc. 120 (1972) 1362.
[56] C. Fang, H. Yakuwa, M. Miyasaka, T. Narita, Oxid. Met. 54 (2000) 173.
[57] J.S. Kirkaldy, G.M. Bolze, D. McCutcheon, D.J. Young, Met. Trans. 4 (1973) 1519.
[58] P.C. Patnaik, W.W. Smeltzer, J. Electrochem. Soc. 131 (1984) 2688.
[59] J. Flahaut, Ann. de Chim. 12e Series 7 (1952) 632.
[60] K. Nishida, T. Narita, Bull. Faculty Eng. Hokkaido Univ. 81 (1976) 99.
[61] T. Murakami, N. Nagasaki, Nippon Zing. Gakk. 4 (1940) 221.
[62] R.B. Setterlund, G.R. Prescott, Corrosion 17 (1961) 277t.
[63] K.N. Strafford, R. Manifold, Oxid. Met. 5 (1972) 85.
[64] K. Nishida, Trans. I.S.I.J. 10 (1970) 421.
[65] P.J. Smith, P.R.S. Jackson, W.W. Smeltzer, J. Electrochem. Soc. 134 (1987) 1424.
[66] P.J. Smith, W.W. Smeltzer, Oxid. Met. 28 (1987) 291.
[67] K. Natesan, Oxid. Met. 30 (1988) 53.
[68] E. Godlewska, K. Godlewski, S. Mrowec, Mat. Sci. Eng. 87 (1987) 183.
[69] S. Mrowec, W. Wedrychowska, Oxid. Met. 13 (1979) 481.
[70] P.D. Zelanko, G. Simkovich, Oxid. Met. 8 (1974) 343.
[71] W.W. Smeltzer, T. Narita, K. Przybylski, in: A.V. Levy (Ed.), Proc. Corrosion Erosion of Materials in Emerging Fossil Energy Systems, NACE, Houston, TX, 1982, p. 860.
[72] T. Biegun, A. Bruckmann, cited in Ref. [9].
[73] K. Nishida, T. Narita, in: Proc. 8th Int. Cong. Metallic Corros., 1, 1981, p. 821.
[74] G. Southwell, D.J. Young, Oxid. Met. 34 (1990) 161.
[75] G. Southwell, D.J. Young, Oxid. Met. 36 (1991) 409.
[76] P. Papaiacovou, H.-P. Schmidt, H. Erhart, H.J. Grabke, Werkst. Korros. 38 (1987) 498.
[77] P. Papaiacovou, H.J. Grabke, P. Schmidt, Werkst. Korros. 36 (1985) 320.
[78] W.W. Smeltzer, D.J. Young, T. Walec, F.A. Elrefaie, in: Proc. 9th Int. Cong. Met. Corros., vol. 2, NRCC, Ottawa, 1984, p. 24.

[79] N.S. Quan, D.J. Young, Oxid. Met. 25 (1986) 107.
[80] Y. Chen, D.J. Young, S. Blairs, Corros. Sci. 36 (1994) 401.
[81] R.V. Carter, D.L. Douglass, F. Gesmundo, Oxid. Met. 31 (1989) 341.
[82] V. Raghavan, Phase Diagrams of Ternary Iron Alloys, Part 2: Ternary Systems Containing Iron and Sulphur, Indian Institute of Metals, Calcutta, 1988, p. 180.
[83] D.J. Young, W.W. Smeltzer, J.S. Kirkaldy, Oxid. Met. 7 (1973) 149.
[84] M.F. Chen, D.L. Douglass, Oxid. Met. 32 (1989) 185.
[85] H. Wada, M. Onoda, H. Nozaki, I. Kawada, J. Less-Common Met. 113 (1985) 53.
[86] M.F. Chen, D.L. Douglass, F. Gesmundo, Oxid. Met. 33 (1990) 399.
[87] G. Wang, D.L. Douglass, F. Gesmundo, Oxid. Met. 35 (1991) 349.
[88] R.Y. Chen, D.J. Young, S. Blairs, Oxid. Met. 54 (2000) 103.
[89] Y.R. He, D.L. Douglass, Oxid. Met. 40 (2003) 119.
[90] Y. Chen, D.J. Young, S. Blairs, Oxid. Met. 40 (1993) 433.
[91] M.F. Chen, D.L. Douglass, F. Gesmundo, Oxid. Met. 31 (1989) 237.
[92] G. Wang, R. Carter, D.L. Douglass, Oxid. Met. 32 (1989) 273.
[93] B. Gleeson, D.L. Douglass, F. Gesmundo, Oxid. Met. 31 (1989) 209.
[94] B. Gleeson, D.L. Douglass, F. Gesmundo, Oxid. Met. 33 (1990) 425.
[95] T. Izumi, T. Yoshioka, S. Hayashi, T. Narita, Intermetallics 8 (2000) 891, 9 (2001) 547.
[96] T. Izumi, T. Yoshioka, S. Hayashi, T. Narita, Intermetallics 10 (2002) 353, 13 (2005) 694.
[97] T. Narita, T. Izumi, M. Yatagai, T. Yoshioka, Intermetallics 8 (2000) 371.
[98] H. Habazaki, K. Hashimoto, S. Mrowec, M. Danielewski, Corros. Sci. 36 (1984) 199.
[99] M. Schutze, M. Malessa, V. Rohr, T. Weber, Surf. Coat. Technol. 201 (2006) 3872.
[100] D. deB Darwent, R. Roberts, Proc. Roy. Soc. London A 216 (1953) 344.
[101] C.D. Holland, R.G. Anthony, Fundamentals of Chemical Reaction Engineering, Prentice-Hall, Englewood Cliffs, NJ, 1979.
[102] J.P. Orchard, D.J. Young, J. Electrochem. Soc. 133 (1986) 1734.
[103] A. Dravnieks, C.H. Samans, J. Electrochem. Soc. 105 (1958) 183.
[104] E.W. Haycock, J. Electrochem. Soc. 106 (1959) 764.
[105] E.T. Turkdogan, Trans. AIME 242 (1968) 1665.
[106] G. Simkovich, Werkst. Korros. 21 (1970) 973.
[107] J.P. Orchard, D.J. Young, J. Electrochem. Soc. 136 (1989) 545.
[108] D.J. Young, J.P. Orchard, Can. Met. Quart. 30 (1991) 227.
[109] R.A. Rapp, Met. Trans. A 15A (1984) 765.
[110] W.H. Cheung, D.J. Young, Oxid. Met. 36 (1991) 15.
[111] K. Przybylski, M. Potoczek (1993), cited in Ref. [10].
[112] F. Gesmundo, F. Viani, K. Godlewski, in: Proc. 7th Asian Pacific Corrosion Control Conference, vol. 1, International Academic Publishers, Beijing, 1991, p. 90.
[113] J.R. Regina, J.N. Dupont, A.R. Marder, Mater. Sci. Eng. A 404 (2005) 71, 405 (2006) 102.
[114] P. Mari, J.P. Chaise, J.P. Larpin, Oxid. Met. 17 (1982) 315.
[115] E.M. Jalloulic, J.P. Larpin, M. Lambertin, J.C. Colson, Oxid. Met. 11 (1979) 335.
[116] F.H. Stott, M.F. Chong, C.A. Stirling, in: Proc. 9th Int. Cong. Met. Corros., NRCC, Ottawa, 1984 vol.2, p.1.
[117] J.K.R. Weber, M.G. Hocking, Oxid. Met. 32 (1989) 1.
[118] W. Kai, D.L. Douglass, F. Gesmundo, Oxid. Met. 37 (1992) 389.
[119] W. Kai, D.L. Douglass, Oxid. Met. 39 (1993) 281.
[120] Y.R. He, D.L. Douglass, Oxid. Met. 40 (1993) 119.
[121] P.F. Tortorelli, J.H. DeVan, Mater. Sci. Eng. A 153 (1992) 573.
[122] J.H. DeVan, P.F. Tortorelli, Corros. Sci. 35 (1993) 1065.

[123] P.F. Tortorelli, K. Natesan, Mater. Sci. Eng. A 258 (1998) 115.
[124] F.Q. Lang, Z.M. Yu, S. Gedevanishvili, S.C. Deevi, S. Hayashi, T. Narita, Intermetallics 12 (2004) 469.
[125] B. Schramm, W. Auer, Mater. Corros. 47 (1996) 678.
[126] E. Godlewska, Mater. Corros. 48 (1997) 687.
[127] K. Natesan, R.N. Johnson, Surf. Coat. Technol. 43−44 (1990) 821.
[128] A.U. Malik, K. Natesan, Oxid. Met. 34 (1990) 497.
[129] W.T. Bakker, Oxid. Met. 45 (1996) 487.
[130] K. Natesan, Mater. High Temp. 14 (1997) 137.
[131] J.H. Swisher, Trans. AIME 242 (1968) 2433.
[132] T. Narita, W.W. Smeltzer, K. Nishida, Oxid. Met. 17 (1982) 299.
[133] J.A. Chitty, W.W. Smeltzer, J. Electrochem. Soc. 120 (1973) 1362.
[134] W. Kai, C.T. Leu, P.Y. Lee, Oxid. Met. 46 (1996) 185.
[135] D.J. Young, S. Watson, Oxid. Met. 44 (1995) 239.
[136] M.A. Harper, J.P. Cotner, Oxid. Met. 53 (2000) 427.
[137] D.A. Shores, W.C. Fang, J. Electrochem. Soc. 128 (1981) 346.
[138] W.C. Fang, R.A. Rapp, J. Electrochem. Soc. 130 (1983) 2335.
[139] J. Stringer, D.P. Whittle, in: Z.A. Foroulis, W.W. Smeltzer (Eds.), Metal-Slag-Gas Reactions and Processes, Electrochemical Soc, Pennington, NJ, 1975, p. 665.
[140] L.D. Paul, R.R. Seeley, Corrosion 47 (1991) 152.
[141] E. Rocca, P. Steinmetz, M. Moliere, J. Eng. Gas Turbines Power 125 (2003) 664.
[142] J. Stringer, Mater. Sci. Technol. 3 (1987) 482.
[143] F.S. Pettit, C.S. Giggins, in: C.T. Sims, N.S. Stoloff, W.C. Hagel (Eds.), Superalloys II, Wiley, New York, 1987, p. 327.
[144] P. Kofstad, High Temperature Corrosion, Elsevier, London, 1988.
[145] R.A. Rapp, in: O. Johannesen, A.G. Andersen (Eds.), Selected Topics in High Temperature Chemistry: Defect Chemistry of Solids, Elsevier, Amsterdam, 1989, p. 291.
[146] R.A. Rapp, Y.S. Zhang, JOM 46 (1994) 47.
[147] N.S. Bornstein, W.P. Allen, Mater. Sci. Forum 251−252 (1997) 127.
[148] E.L. Simons, G.V. Browning, H.A. Liebhafsky, Corrosion 11 (1955) 505.
[149] A.U. Seybolt, Trans. AIME 242 (1968) 1955.
[150] N.S. Bornstein, M.A. De Crescente, Trans. AIME 245 (1969) 1947.
[151] N.S. Bornstein, M.A. De Crescente, Corrosion 26 (1970) 209.
[152] N.S. Bornstein, M.A. De Crescente, Met. Trans. 2 (1971) 2875.
[153] J.A. Goebel, F.S. Pettit, Met. Trans. 1 (1970) 1943.
[154] J.A. Goebel, F.S. Pettit, G.W. Goward, Met. Trans. 4 (1973) 261.
[155] C.O. Park, R.A. Rapp, J. Electrochem. Soc. 133 (1986) 1636.
[156] J.M. Quets, W.H. Dresker, J. Mater. 4 (1969) 583.
[157] K.A. Bolshakov, P.T. Federov, Zh. Neorg. Khim 3 (1958) 1896.
[158] D.K. Gupta, R.A. Rapp, J. Electrochem. Soc. 127 (1980) 2194.
[159] Y.S. Zhang, R.A. Rapp, J. Electrochem. Soc. 132 (1985) 734, 2498.
[160] Y.S. Zhang, J. Electrochem. Soc. 133 (1986) 655.
[161] P.D. Jose, D.K. Gupta, R.A. Rapp, J. Electrochem. Soc. 132 (1985) 735.
[162] D.Z. Shi, R.A. Rapp, J. Electrochem. Soc. 133 (1986) 849.
[163] M.L. Deanhardt, K.H. Stern, J. Electrochem. Soc. 128 (1981) 2577, 129 (1982) 2228.
[164] A.K. Misra, D.P. Whittle, W.L. Worrell, J. Electrochem. Soc. 129 (1982) 1840.
[165] R.A. Rapp, K.S. Goto, in: J. Braunstein, J.R. Selman (Eds.), Molten Salts I, Electrochemical Society, Pennington, NJ, 1981, p. 159.

[166] N. Otsuka, R.A. Rapp, J. Electrochem. Soc. 137 (1990) 46.
[167] D.A. Shores, in: R.A. Rapp (Ed.), High Temperature Corrosion, NACE, Houston, TX, 1983, p. 493.
[168] K. Luthra, D.A. Shores, J. Electrochem. Soc. 127 (1980) 2202.
[169] K. Luthra, J. Electrochem. Soc. 132 (1985) 1293.
[170] L.Q. Shi, Y.S. Zhang, S.T. Shih, Corros. Sci. 33 (1992) 1427.
[171] L.Q. Shi, Y.S. Zhang, S.T. Shih, Oxid. Met. 38 (1992) 385.
[172] J.R. Nicholls, D.J. Stephenson, Corros. Sci. 33 (1992) 1313.
[173] A. Rahmel, M. Schmidt, M. Schorr, Oxid. Met. 18 (1982) 195.
[174] W.T. Wu, A. Rahmel, M. Schorr, Oxid. Met. 22 (1984) 59.
[175] G.W. Goward, Surf. Coat. Technol. 108 (1998) 73.
[176] D.R. Clarke, C.G. Levy, Ann. Rev. Mater. Res. 33 (2003) 383.
[177] E.J. Felten, Oxid. Met. 10 (1976) 23.
[178] G.H. Meir, F.S. Pettit, Surf. Coat. Technol. 39/40 (1989) 1.
[179] V. Deodeshmukh, B. Gleeson, Corrosion 2006, NACE, Houston, TX, 2006. Paper 06476.
[180] G.J. Tatlock, T.J. Hurd, Werkst. Korros. 41 (1990) 710.
[181] J.R. Nicholls, N.J. Simms, W. Chan, H.E. Evans, Surf. Coat. Technol. 149 (2002) 236.
[182] V. Deodeshmukh, N. Mu, B. Li, B. Gleeson, Surf. Coat. Technol. 201 (2006) 3836.
[183] Y.N. Wu, A. Yamaguchi, H. Murakami, S. Kuroda, J. Mater. Res. 22 (2007) 206.
[184] A. Naji, M.C. Galetz, M. Schuetze, Mater. Corros. 65 (2014) 312.
[185] R.J. Bennett, R. Krakow, A.S. Eggeman, C.N. Jones, H. Murakami, C.M.F. Rae, Acta Mat. 92 (2015) 278.